Band properties of the transitional nucleus ^{187}Pt

X. H. Zhou,[1,2] Y. B. Xing,[1,2] M. L. Liu,[1] Y. H. Zhang,[1] Y. X. Guo,[1] L. Ma,[1] X. G. Lei,[1] and W. T. Guo[1]
[1]*Institute of Modern Physics, Chinese Academy of Sciences, Lanzhou 730000, People's Republic of China*
[2]*Graduate School of the Chinese Academy of Sciences, Beijing 100049, People's Republic of China*

M. Oshima, Y. Toh, M. Koizumi, A. Osa, and Y. Hatsukawa
Japan Atomic Energy Agency, Tokai, Ibaraki 319-1195, Japan

F. R. Xu
Department of Technical Physics and MOE Key Laboratory, Peking University, Beijing 100871, People's Republic of China

M. Sugawara
Chiba Institute of Technology, Narashino, Chiba 275-0023, Japan
(Received 11 December 2006; published 26 March 2007)

High-spin states in ^{187}Pt have been studied experimentally using the ^{173}Yb(^{18}O, 4n) reaction at beam energies of 78 and 85 MeV. The previously known bands based on the $\nu i_{13/2}$, $\nu 7/2^-[503]$, and $\nu i_{13/2}^2 \nu j$ configurations have been extended to high-spin states, and new rotational bands associated with the $\nu 3/2^-[512]$ and $\nu 1/2^-[521]$ Nilsson orbits have been identified. The total Routhian surface calculations indicate that the transitional nucleus ^{187}Pt is very soft with respect to β and γ deformations. The band properties, such as level spacings, band crossing frequencies, alignment gains, and signature splittings, have been compared with the systematics observed in neighboring nuclei and have been interpreted within the framework of the cranked shell model. The rotational bands show different band crossing frequencies, which can be explained by the alignment either of $i_{13/2}$ neutrons or of $h_{9/2}$ protons. Importantly, evidence is presented for a $\pi h_{9/2}$ alignment at very low frequency in the $\nu 7/2^-[503]$ band. The proton nature of the band crossing is strongly suggested by comparing the measured $B(M1; I \rightarrow I-1)/B(E2; I \rightarrow I-2)$ ratios with the theoretical values from the semiclassical Dönau and Frauendof approach.

DOI: 10.1103/PhysRevC.75.034314 PACS number(s): 21.10.Re, 23.20.Lv, 25.70.Gh, 27.70.+q

I. INTRODUCTION

The neutron-deficient Pt-Hg nuclei are well known to exhibit shape coexistence phenomenon [1,2], and this has provided the motivation for extensive studies both experimentally and theoretically. Different structures associated with prolate, oblate, and triaxial shapes within the same nucleus have been identified experimentally [1,2], and the ground-state shape transitions for the isotopic chains have been observed [3–5]. In the even-A Pt isotopes from $A = 170$ to $A = 190$ [2,6,7], nuclear structure studies have presented strong evidence for the shape coexistence at low energy; the isotope shift measurements have shown a sharp change of the nuclear charge radius between ^{188}Pt and ^{186}Pt [3–5], suggesting a ground-state shape transition from the near oblate shape for the Pt nuclei with $A \geqslant 188$ to the prolate shape for $A \leqslant 186$. Therefore, the spectroscopic information of ^{187}Pt is of particular interest as it lies between the two nuclei ^{186}Pt and ^{188}Pt where the change in collective structure should be most drastic. One expects that rotational bands with different shapes should coexist in ^{187}Pt. Due to the pronounced transitional character, the nucleus ^{187}Pt would be rather soft with respect to β and γ deformations, and the shape-polarizing effects arising from valence nucleons and aligned quasiparticles associated with band crossings might be significant. In this article, it is our primary aim to extend the level scheme of ^{187}Pt to high-spin states via heavy-ion induced reaction and to study the shape coexistence phenomenon.

For the Ir-Pt-Au nuclei with neutron number $N = 106$–108 [8–15], there exists a very interesting phenomenon concerning the nature of the band crossing. The first band crossing for the neutron-deficient prolate Ir-Pt-Au nuclei with neutron number less than 106 clearly results from the alignment of a pair of $i_{13/2}$ quasineutrons. However, there has been much debate about the nature of the first crossing at $N = 106$–108 [8–15]. In these isotopes, the rotational bands, not involving $i_{13/2}$ neutrons or $h_{9/2}$ protons, show at least one, but in certain cases two, distinguishable band crossings below $\hbar\omega \approx 0.35$ MeV [8–15]. These bands have been observed experimentally up to very high frequencies, and the alignment gain after the band crossing approaches $10.0\hbar$. The observed band crossings and alignment gains have been explained successfully using two very different scenarios [8]. In the first scenario, it is assumed that all the bands have similar deformations, and therefore standard blocking arguments were used. The conclusion is that the alignment of $h_{9/2}$ protons plays a crucial role at frequencies below 0.35 MeV [8]. In the second scenario, the band crossings have been interpreted to be deformation dependent. The cranked-shell-model (CSM) calculations show that a given band crossing might appear at very different frequency depending on the deformation of the considered configuration [8–10]. Thus, nearly all band crossings are explained as the alignment of $i_{13/2}$ neutrons, and the alignment of $h_{9/2}$ protons is responsible for only exceptional cases [8]. To settle this dispute, detailed experimental information concerning the

 ©2007 The American Physical Society

band properties is needed. As well known, the ratios of reduced transition probabilities $B(M1; I \rightarrow I-1)/B(E2; I \rightarrow I-2)$ are sensitive to the quasiparticle configurations below and above the band crossing. Because of the opposite signs of the proton versus neutron g factors, the proton alignment in a band based on neutron configuration usually results in an increase in the $B(M1)$ value, whereas a neutron alignment has the opposite effect. The converse is also true for a band associated with proton configuration. With the modern powerful γ detector array, we can obtain very high statistical data from which precise $B(M1; I \rightarrow I-1)/B(E2; I \rightarrow I-2)$ ratios can be extracted. This could help us to classify the nature of the low-frequency band crossings in the Ir-Pt-Au nuclei with neutron number around 108.

Prior to this work, the ground state of ^{187}Pt was proposed to be the $3/2^-[512]$ Nilsson configuration [3]. Detailed knowledge of low-spin states in ^{187}Pt was provided from decay studies of ^{187}Au [16–18]. Particularly, spin values were firmly assigned to many low-lying levels in ^{187}Pt, and Nilsson configurations with prolate and oblate shapes were tentatively suggested to the excited states [16–18]. In an α-induced reaction [19], the $\nu i_{13/2}$ band was identified for ^{187}Pt. Rotational bands built on the $\nu i_{13/2}$ and $\nu 7/2^-[503]$ configurations in ^{187}Pt were observed to moderate high-spin states and were reported in an annual report [20]. However, a detailed high-spin level scheme of ^{187}Pt has not yet been published in the literature so far.

In this article, we report experimental results on high-spin structures in ^{187}Pt. The experimental details and data analysis will be described in Sec. II. The experimental quantities in the rotating frame and the theoretical calculations to understand the observed properties are presented in Secs. III and IV, respectively. In Sec. V, the configuration assignments to the rotational bands are suggested on the basis of the measured in-band $B(M1)/B(E2)$ ratios and the existing knowledge of band properties in neighboring odd-neutron nuclei. Band properties of the crossing frequencies, alignment gains, and signature splittings are discussed with an emphasis on the nature of band crossings. Concluding remarks are presented in Sec. VI.

II. EXPERIMENTS AND RESULTS

A. Measurements

The excited states in ^{187}Pt were populated via the ^{173}Yb(^{18}O, $4n$) reaction. The $^{18}O^{7+}$ beam was provided by the tandem accelerator at the Japan Atomic Energy Agency (JAEA). The target was an isotopically enriched ^{173}Yb metallic foil of 2.0 mg/cm^2 thickness with a 7.0-mg/cm^2 Pb backing. The GEMINI [21] γ-ray detector array was used. At the time of this experiment, an array consisting of 13 hyperpure germanium detectors with bismuth germanate anti-Compton (AC) shields was used; 6 detectors had an efficiency of 40% each and the others had 70% relative to $3'' \times 3''$ NaI. The detectors were calibrated with ^{60}Co, ^{133}Ba, and ^{152}Eu standard sources; the typical energy resolution was about 2.0–2.4 keV at full width half maximum (FWHM) for the 1332.5-keV line. Due to the location of the compound nucleus ^{191}Pt in the proximity of the stability line, neutron evaporation channels were dominant for the present projectile and target combination. To get information for identifying the in-beam γ rays belonging to ^{187}Pt, X-γ-t and γ-γ-t coincidence measurements were performed at beam energies of 78 and 85 MeV, at which energies the yields of ^{187}Pt were large. Here, t refers to the relative time difference between any two coincident γ rays detected within $\pm$200 ns. During the coincidence measurements, the beam intensity of about 1.5 pnA was maintained, at which the γ-γ coincidence counting rate was about 1800 per second. A total of 240×10^6 coincidence events were accumulated. After accurate gain matching, these coincidence events were sorted into a symmetric matrix for off-line analysis.

To obtain the DCO (Directional Correlations of γ rays deexciting the Oriented states) ratios, the detectors were divided into three groups, of which the angle positions (and detector number at that angle) were $\pm 40^\circ(6)$, $\pm 58^\circ(2)$, and $90^\circ(5)$ with respect to the beam direction. A nonsymmetrized matrix with detectors at $\theta_2 = 90^\circ$ against those at $\theta_1 = \pm 40^\circ$ was constructed. The experimental DCO ratio was calculated by $R_{\rm DCO}(\gamma) = I_\gamma(\theta_1)/I_\gamma(\theta_2)$, where $I_\gamma(\theta_1)$ represents the intensity of an unknown γ ray along the θ_1 axis in coincidence with the stretched $E2$ transition along θ_2 direction. Similarly, with the same gate on θ_1 axis, coincidence spectrum along the θ_2 axis was projected to determine $I_\gamma(\theta_2)$. In the present geometry, stretched quadrupole transitions were adopted if $R_{\rm DCO}(\gamma)$ ratios were close to unity, and dipole transitions were assumed if $R_{\rm DCO}(\gamma) \approx 0.7$. Additionally, to extract information concerning γ-ray anisotropies, the coincidence data were sorted into two asymmetric matrices whose x-axis was the γ-ray energy deposited in the detectors at any angles and y-axis was the γ-ray energy deposited in the detectors at $\pm 40^\circ$ and 90°, respectively. By gating on the x-axis with suitable γ rays, two spectra measured at $\pm 40^\circ$ and 90° angle positions were obtained. After correcting for the overall detection efficiency of the detectors at each of the two angles and normalizing the two spectra with respect to each other, γ-ray anisotropy ($R_{\rm ADO}(\gamma)$) was deduced from the intensity ratio in the two spectra. Typical γ-ray anisotropies for the known γ rays observed in this experiment were 1.3 for stretched quadrupole transitions and 0.7 for stretched pure dipole transitions. Therefore, we assigned the stretched quadrupole transition and stretched dipole transition to the γ rays of ^{187}Pt with anisotropies around 1.3 and 0.7, respectively.

B. Level scheme

Extensive decay studies of ^{187}Au established many low-lying states in ^{187}Pt with spin values firmly assigned [16,17, 20]. This provided important basis for the present in-beam work because rotational bands were suggested to be built on some of the low-lying states observed in the decay work [16,17]. Assignments of the observed new γ rays to ^{187}Pt were based on the coincidences with the known γ rays [16,17]. The measured relative γ-ray yields at different beam energies, combined with Pt K x-ray coincident information, gave us additional information to assign new γ-ray cascades

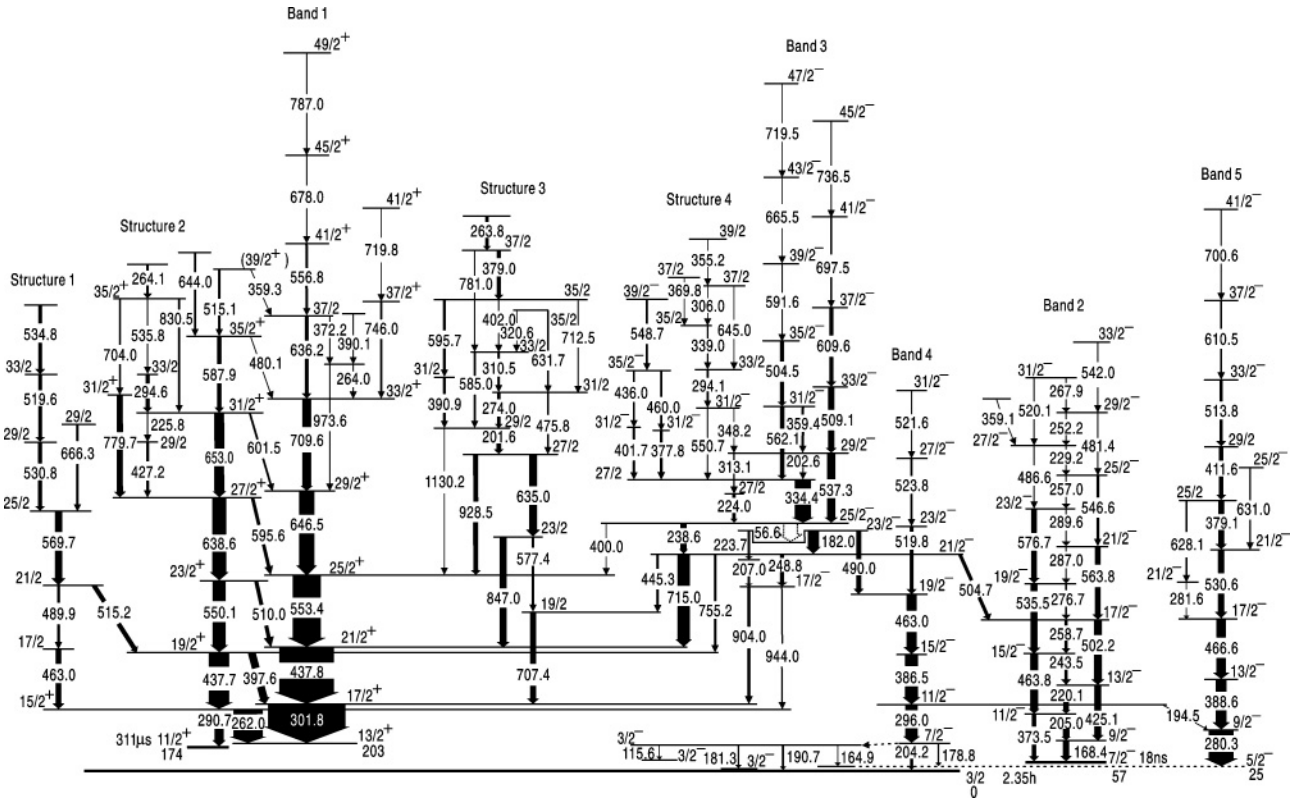

FIG. 1. Level scheme of ^{187}Pt deduced from the present work. The widths of the arrows indicate the relative transition intensities.

to ^{187}Pt. Gated spectrum was produced for each of the γ rays assigned to ^{187}Pt. Based on the analysis of γ-γ coincidence relationships, a complicated level scheme for ^{187}Pt has been proposed and presented in Fig. 1. The ordering of transitions in the level scheme was determined according to the γ-ray relative intensities, γ-γ coincidence relationships, and γ-ray energy sums. The transition character was deduced from the measured DCO and γ-ray anisotropy results. In assigning spins and parities to the observed levels, we have assumed that stretched quadrupole transitions are of $E2$ multipolarity and that the pure dipoles can have either $E1$ or $M1$ character as well as that the mixed transitions are of $M1/E2$ type. The spins and parities for the known low-lying states were adopted from the previous work [16,17,20], and these values were used as the references of the spin and parity assignments for the high-spin states. In the present work, we have used the general yrast argument that levels populated in heavy-ion reactions usually have spins increasing with increasing excitation energy. Therefore, the measured DCO and γ-ray anisotropy results allow straightforward determinations of spins and parities for the excited states in ^{187}Pt. Some brief explanations of the level scheme are given as follows.

Band 1 was populated most strongly, and the order of transitions was fixed firmly with the observation of in-band transitions. This band was observed previously, and suggested to be associated with the $\nu i_{13/2}$ configuration [19,20]. The $11/2^+$ and $13/2^+$ band head energies were determined to be 174 and 203 keV [16–18], respectively. The $11/2^+$ state was identified to be a long-lived isomer [17,18]. In the present work, this band has been extended up to $I^\pi = 49/2^+$ for the $\alpha = +1/2$ sequence and $I^\pi = 39/2^+$ for the $\alpha = -1/2$ sequence, and the transitions from the unfavored signature to the favored signature have been observed. As shown in Fig. 1, several structures feed band 1 at different spins. With the existence of parallel decay pathways and many crossover transitions, the positions of these structures in the level scheme are rather firm. For example, the 928.5-keV transition is in coincidence with the 553.4-, 437.8-, and 301.8-keV transitions. The parallel cascade of 635.0- and 847.0-keV transitions is in coincidence with the 437.8- and 301.8-keV transitions but not with the 553.4-keV transition, whereas the 577.4- and 707.4-keV transitions show coincidence only with the 301.8-keV transition. These coincidence patterns, together with energy sum relationships of the involved transitions, firmly established the locations of the 707.4-, 577.4-, 847.0-, 635.0-, and 928.5-keV transitions in the level scheme. Gated spectra demonstrating the existence of band 1 and the associated structures are shown in Figs. 2 and 3.

Band 2 is built on the 57-keV state. In the previous studies [16–18], the $I^\pi = 7/2^-$57-keV isomeric level with a half-life-of 18.0 ns was observed, and a coupled rotational band based on this isomer was established [20]. A γ-ray spectrum gated on the 168.4-keV transition is shown in Fig. 4. The 31.6-keV transition, suggested to depopulate the 57-keV isomer [19,20], was not observed in the present work because of its highly converted nature and low detection efficiency. The present data extend this band from $I^\pi = 17/2^-$ to $I^\pi = 33/2^-$.

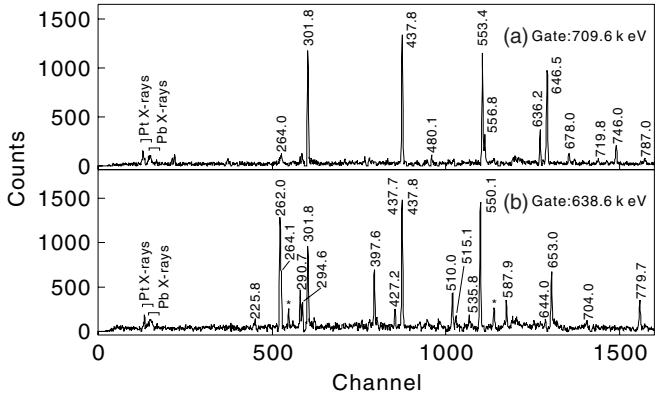

FIG. 2. The γ-ray spectra gated on the (a) 709.6-keV transition and (b) 638.6-keV transition. The asterisks indicate contaminations.

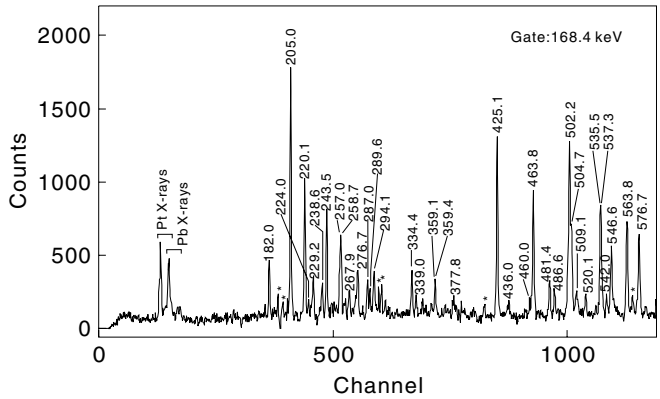

FIG. 4. The γ-ray spectrum gated on the 168.4-keV transition. The asterisks indicate contaminations.

Band 3 should be based on a three quasiparticle state. In the α-induced reaction [19], a cascade consisting of the 715.0-, 182.0-, and 334.4-keV transitions was observed to feed the $21/2^+$ level of band 1. The spin and parity of the state depopulated by the 715.0-keV transition were tentatively proposed to be $21/2^-$ [19]. The measured DCO and ADO ratios for the 715.0-keV transition indicate it to be a stretched quadrupole transition or transition connecting levels with same spin values. Therefore, we propose that the level depopulated by the 715.0-keV transition should have spin and parity of either $21/2^{\pm}$ or $25/2^+$. Considering the observation of a parallel 755.2-keV transition feeding the $19/2^+$ level of band 1, we prefer the assignment of $21/2^{\pm}$. Otherwise, the 755.2-keV transition should have an $M3$ multipolarity, and it could not compete with the 715.0-keV transition. Based on the systematic observation of a $21/2^-$ level at similar energy in the neighboring nuclei [19], we propose spin and parity of $21/2^-$ for the state decaying by the 715.0-keV transition. A rotational band, associated with this $21/2^-$ state, has been observed up to high-spin states and numbered as band 3. Gated spectra showing the existence of band 3 and its decay paths are shown in Fig. 5. Transitions between the two signatures were observed only at the bottom of band 3. The 182.0-keV transition shows strong coincidence with the transitions above the $23/2^-$ level. Therefore, we assume that there exists a 56.6-keV transition connecting the $23/2^-$ and $25/2^-$ states. This low-energy transition was not observed experimentally due to its highly converted nature and low detection efficiency. If band 3 is proposed to be built on the $21/2^-$ state, there would exist a 391.0-keV $E2$ transition between the $27/2^-$ and $23/2^-$ band members. However, we have not observed this expected in-band $E2$ transition. One explanation for the missing 391.0-keV transition is that band 3 might build on the $25/2^-$ state, which was favored by the decay patterns shown in Fig. 1. Several transitions feed the $27/2^-$ state depopulated by the 334.4-keV transition.

Band 4 is built on the ground state. This band was newly established in the present work. It consists of the 204.2-, 296.0-, 386.5-, 463.0-, 519.8-, 523.8-, and 521.6-keV transitions. The 490.0-keV transition is in strong coincidence with the 204.2-, 296.0-, 386.5-, and 463.0-keV transitions but not with the higher-lying transitions in band 4. This fixed the level energies of band 4, and the 204.2-keV transition should directly feed the ground state. Gated spectrum displaying band 4 is shown in Fig. 6. The ground state of ^{187}Pt was proposed to be the $3/2^-[512]$ Nilsson orbit [3]. Angular correlations and anisotropies suggested $\Delta I = 2$ character for the transitions in band 4. Spins and parities are therefore assigned to the band members. As shown in Fig. 6, the transitions above the 204.2-keV transition show evident coincidences with the

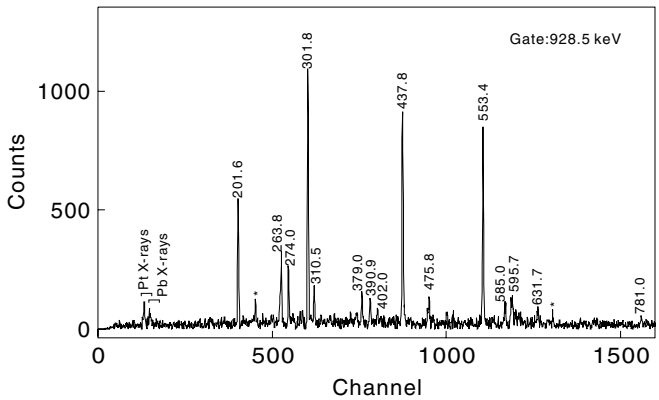

FIG. 3. The γ-ray spectrum gated on the 928.5-keV transition. The asterisks indicate contaminations.

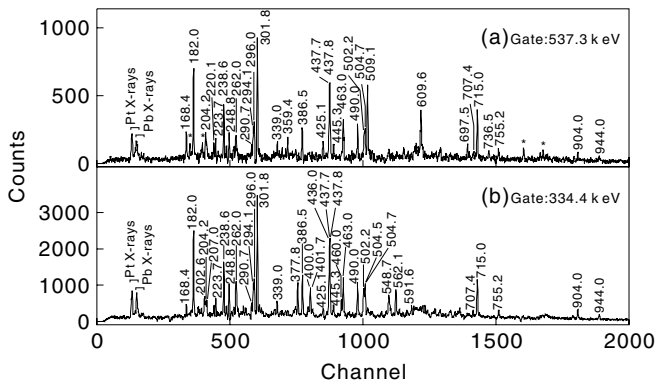

FIG. 5. The γ-ray spectra gated on the (a) 537.3-keV transition and (b) 334.4-keV transition. The asterisks indicate contaminations.

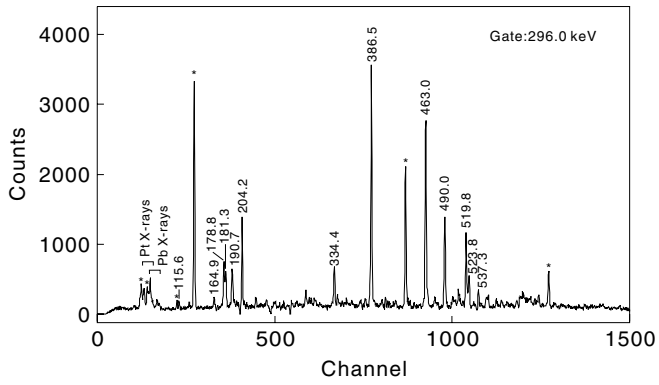

FIG. 6. The γ-ray spectrum gated on the 296.0-keV transition. The asterisks indicate contaminations mainly from ^{186}Os.

115.6-, 181.3-, 164.9-, and 190.7-keV transitions observed in the decay studies [16–18], indicating the existence of a nonobserved low-energy transition between the 204.2- and 190.7-keV states.

Band 5 has a typical character of decoupled band. This band was newly established in the present work. A γ-ray spectrum gated on the 530.6-keV transition is shown in Fig. 7. Angular correlations and anisotropies for the transitions in the cascade are consistent with $\Delta I = 2$ character. As shown in Fig. 7, the 194.5-keV transition is in clear coincidence with the 280.3-keV transition but not with the others in band 5. Based on analysis of coincidence relationships, we propose that the 194.5-keV transition should link the $11/2^-$ level of band 4 and the level depopulated by the 280.3-keV transition. This results in an excitation energy of 25.0 keV for the level populated by the 280.3-keV transition. A 25.0-keV state with $I^\pi = 5/2^-$ was observed in the previous decay work [16–18]. We propose that band 5 is built on this state. Additionally, the 178.8-keV transition was observed to be in coincidence with the transitions above the $7/2^-$ level of band 4, and its energy is exactly equal to the energy difference between the $7/2^-$ level

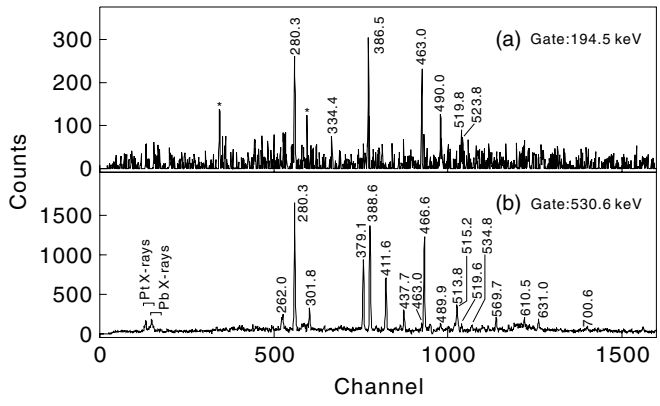

FIG. 7. The γ-ray spectra gated on the (a) 194.5-keV transition and (b) 530.6-keV transition. Note that there is a 530.8-keV transition in structure 1, and the transitions in structure 1 appear in the spectrum gated by the 530.6-keV transition. The asterisks indicate contaminations.

of band 4 and the $5/2^-$ level of band 5. We propose that the 178.8-keV transition likely connects these two levels.

C. Experimental transition probabilities

For the $\Delta I = 1$ rotational bands shown in Fig. 1, the branching ratios, which are defined as

$$\lambda = \frac{T_\gamma(I \to I-2)}{T_\gamma(I \to I-1)}, \tag{1}$$

were extracted for most transitions. Here $T_\gamma(I \to I-2)$ and $T_\gamma(I \to I-1)$ are the γ-ray intensities of the $\Delta I = 2$ and $\Delta I = 1$ transitions, respectively. These intensities are measured in a summed coincidence spectrum gated by the transitions above the state of interest. The branching ratios were used to extract the reduced transition probability ratios, which are defined as [22]

$$\frac{B(M1; I \to I-1)}{B(E2; I \to I-2)} = 0.697 \frac{[E_\gamma(I \to I-2)]^5}{[E_\gamma(I \to I-1)]^3} \frac{1}{\lambda} \times \frac{1}{1+\delta^2} \left(\frac{\mu_N^2}{e^2 b^2}\right), \tag{2}$$

where δ is the $E2/M1$ mixing ratio for the $\Delta I = 1$ transitions and $E_\gamma(I \to I-1)$ and $E_\gamma(I \to I-2)$ are the $\Delta I = 1$ and $\Delta I = 2$ transition energies, respectively. The mixing ratio δ deduced from angular correlation coefficients in the neighboring odd-N isotopes varies between 0.0 and 0.3 [9]. This small value has little effect on the extracted reduced transition probability ratios. Consequently, the value $\delta = 0.0$ has been used in the present analysis.

The relative intensities for some uncontaminated γ rays could be measured in the total projection spectrum. Most of the relative intensities were extracted from the spectra gated on the bottom transitions in the band. The relative intensities are corrected with the detection efficiencies. The γ-ray energies, spin and parity assignments, relative γ-ray intensities, branching ratios λ, extracted $B(M1)/B(E2)$ values, DCO ratios $R_{\rm DCO}(\gamma)$, and anisotropies $R_{\rm ADO}(\gamma)$ are presented in Table I grouped in sequences for each band.

III. EXPERIMENTAL ROUTHIANS AND ALIGNMENTS

For a rotational band, the nature of intrinsic state and aligned quasiparticles associated with band crossing is reflected in the band properties, such as the aligned angular momentum, the band crossing frequency, and the gain of alignment after band crossing. To compare the experimental results with the calculations described below, we must transform the experimental excitation energies and spins into the rotating frame. The standard plots of the quasiparticle aligned angular momenta (i) and Routhians (e) as functions of rotational frequency are shown in Fig. 8. Each of these quantities is extracted from measured spins, level energies, and transition energies. The quasiparticle aligned angular momentum results from the subtraction of a reference angular momentum, $\omega J_0 + \omega^3 J_1$, from the total angular momentum along the rotational axis [23]; the Routhian is calculated by subtracting a reference energy, $-\frac{1}{2}\omega^2 J_0 - \frac{1}{4}\omega^4 J_1 + \frac{1}{8} J_0$, from the total

TABLE I. γ-ray transition energies, spin and parity assignments, γ-ray intensities, branching ratios, extracted $B(M1)/B(E2)$ ratios, DCO ratios, and γ-ray anisotropies in ^{187}Pt.

$E\gamma$(keV)[a]	$J_i^\pi \rightarrow J_f^\pi$[b]	I_γ[c]	λ[d]	$B(M1)/B(E2)$[e]	R_{DCO}	R_{ADO}
Band 1						
290.7	$\frac{15}{2}^+ \rightarrow \frac{11}{2}^+$	119			1.07(8)	1.25(11)
437.7	$\frac{19}{2}^+ \rightarrow \frac{15}{2}^+$	263			0.94(7)	1.20(6)
550.1	$\frac{23}{2}^+ \rightarrow \frac{19}{2}^+$	168			1.06(12)	1.30(10)
638.6	$\frac{27}{2}^+ \rightarrow \frac{23}{2}^+$	177			1.02(12)	1.24(15)
653.0	$\frac{31}{2}^+ \rightarrow \frac{27}{2}^+$	128			1.09(11)	1.24(7)
587.9	$\frac{35}{2}^+ \rightarrow \frac{31}{2}^+$	55			1.00(19)	1.32(21)
515.1	$(\frac{39}{2}^+) \rightarrow \frac{35}{2}^+$	30				
262.0	$\frac{15}{2}^+ \rightarrow \frac{13}{2}^+$	381			0.50(4)	0.52(15)
397.6	$\frac{19}{2}^+ \rightarrow \frac{17}{2}^+$	100			0.35(4)	0.36(4)
510.0	$\frac{23}{2}^+ \rightarrow \frac{21}{2}^+$	50			0.46(16)	0.41(7)
595.6	$\frac{27}{2}^+ \rightarrow \frac{25}{2}^+$	43			0.38(8)	0.64(10)
601.5	$\frac{31}{2}^+ \rightarrow \frac{29}{2}^+$	26				
480.1	$\frac{35}{2}^+ \rightarrow \frac{33}{2}^+$	10				
359.3	$(\frac{39}{2}^+) \rightarrow \frac{37}{2}^+$	10				
301.8	$\frac{17}{2}^+ \rightarrow \frac{13}{2}^+$	1000			1.13(3)	1.23(3)
437.8	$\frac{21}{2}^+ \rightarrow \frac{17}{2}^+$	706			0.93(5)	1.21(5)
553.4	$\frac{25}{2}^+ \rightarrow \frac{21}{2}^+$	362			0.97(5)	1.27(6)
646.5	$\frac{29}{2}^+ \rightarrow \frac{25}{2}^+$	196			0.94(9)	1.23(11)
709.6	$\frac{33}{2}^+ \rightarrow \frac{29}{2}^+$	116			0.99(10)	1.19(8)
636.2	$\frac{37}{2}^+ \rightarrow \frac{33}{2}^+$	46			0.96(21)	1.19(12)
556.8	$\frac{41}{2}^+ \rightarrow \frac{37}{2}^+$	30			1.15(25)	1.34(17)
678.0	$\frac{45}{2}^+ \rightarrow \frac{41}{2}^+$	16				1.27(26)
787.0	$\frac{49}{2}^+ \rightarrow \frac{45}{2}^+$	13				1.36(29)
973.6	$\rightarrow \frac{29}{2}^+$	13				
372.2	$\frac{37}{2}^+ \rightarrow$	8				
264.0	$\rightarrow \frac{33}{2}^+$	17				
390.1		9				
746.0	$\frac{37}{2}^+ \rightarrow \frac{33}{2}^+$	26			0.97(29)	1.23(20)
719.8	$\frac{41}{2}^+ \rightarrow \frac{37}{2}^+$	8				1.37(35)
Structure 1						
463.0	$\frac{17}{2} \rightarrow \frac{15}{2}^+$	74			0.35(8)	0.45(6)
489.9	$\frac{21}{2} \rightarrow \frac{17}{2}$	36				1.39(34)
569.7	$\frac{25}{2} \rightarrow \frac{21}{2}$	94			0.98(15)	1.44(31)
530.8	$\frac{29}{2} \rightarrow \frac{25}{2}$	50			1.17(20)	1.45(26)
519.6	$\frac{33}{2} \rightarrow \frac{29}{2}$	48			1.19(41)	1.57(28)
534.8	$\rightarrow \frac{33}{2}$	47				
515.2	$\frac{21}{2} \rightarrow \frac{19}{2}^+$	60			0.41(6)	0.41(6)
666.3	$\frac{29}{2} \rightarrow \frac{25}{2}$	31			0.97(34)	1.26(28)
Structure 2						
779.7	$\frac{31}{2}^+ \rightarrow \frac{27}{2}^+$	78			0.89(15)	1.19(13)
704.0	$\frac{35}{2}^+ \rightarrow \frac{31}{2}^+$	22			1.05(58)	1.63(50)
427.2	$\frac{29}{2} \rightarrow \frac{27}{2}^+$	35			0.71(25)	0.51(14)
225.8	$\frac{31}{2}^+ \rightarrow \frac{29}{2}$	12				
294.6	$\frac{33}{2} \rightarrow \frac{31}{2}^+$	52			0.60(10)	0.60(7)

TABLE I. *(Continued).*

$E\gamma$(keV)[a]	$J_i^\pi \rightarrow J_f^\pi$[b]	I_γ[c]	λ[d]	$B(M1)/B(E2)$[e]	R_{DCO}	R_{ADO}
535.8	$\frac{35}{2}^+ \rightarrow \frac{33}{2}$	10			0.34(9)	0.61(26)
264.1	$\rightarrow \frac{35}{2}^+$	30				
830.5	$\frac{35}{2}^+ \rightarrow \frac{31}{2}^+$	24				
644.0	$\rightarrow \frac{35}{2}^+$	26				
Structure 3						
1130.2	$\frac{29}{2} \rightarrow \frac{25}{2}^+$	11			0.87(21)	1.13(20)
390.9	$\frac{31}{2} \rightarrow \frac{29}{2}$	33				0.80(21)
595.7	$\frac{35}{2} \rightarrow \frac{31}{2}$	34				
847.0	$\frac{23}{2} \rightarrow \frac{21}{2}^+$	87			0.43(5)	0.58(6)
928.5	$\frac{27}{2} \rightarrow \frac{25}{2}^+$	62			0.37(5)	0.48(6)
585.0	$\frac{33}{2} \rightarrow \frac{29}{2}$	24				
781.0	$\frac{37}{2} \rightarrow \frac{33}{2}$	15				
263.8	$\rightarrow \frac{37}{2}$	45				
201.6	$\frac{29}{2} \rightarrow \frac{27}{2}$	61			1.49(20)	1.62(12)
274.0	$\frac{31}{2} \rightarrow \frac{29}{2}$	46			1.54(22)	1.59(20)
310.5	$\frac{33}{2} \rightarrow \frac{31}{2}$	31			0.68(12)	0.88(23)
402.0	$\frac{35}{2} \rightarrow \frac{33}{2}$	15				0.73(30)
379.0	$\frac{37}{2} \rightarrow \frac{35}{2}$	53			0.50(18)	0.42(14)
320.6	$\frac{35}{2} \rightarrow \frac{33}{2}$	11				0.95(32)
707.4	$\frac{19}{2} \rightarrow \frac{17}{2}^+$	79			0.30(6)	0.50(4)
577.4	$\frac{23}{2} \rightarrow \frac{19}{2}$	31				1.19(23)
635.0	$\frac{27}{2} \rightarrow \frac{23}{2}$	103				1.18(12)
475.8	$\frac{31}{2} \rightarrow \frac{27}{2}$	20				1.54(31)
631.7	$\frac{35}{2} \rightarrow \frac{31}{2}$	21				1.29(19)
712.5	$\frac{35}{2} \rightarrow \frac{31}{2}$	13			1.21(62)	1.26(51)
Band 2						
373.5	$\frac{11}{2}^- \rightarrow \frac{7}{2}^-$	56	0.66(5)	0.89(7)	1.06(18)	1.24(23)
463.8	$\frac{15}{2}^- \rightarrow \frac{11}{2}^-$	102	2.49(20)	0.42(3)	1.09(17)	1.22(13)
535.5	$\frac{19}{2}^- \rightarrow \frac{15}{2}^-$	87	3.95(38)	0.37(3)	1.16(21)	1.34(13)
576.7	$\frac{23}{2}^- \rightarrow \frac{19}{2}^-$	70	7.00(81)	0.26(3)	0.92(17)	1.45(19)
486.6	$\frac{27}{2}^- \rightarrow \frac{23}{2}^-$	8	2.67(45)	0.59(10)		1.43(30)
520.1	$\frac{31}{2}^- \rightarrow \frac{27}{2}^-$	8				1.46(36)
168.4	$\frac{9}{2}^- \rightarrow \frac{7}{2}^-$	81			0.65(9)	0.56(3)
205.0	$\frac{11}{2}^- \rightarrow \frac{9}{2}^-$	85			0.57(7)	0.59(4)
220.1	$\frac{13}{2}^- \rightarrow \frac{11}{2}^-$	72			0.61(6)	0.61(7)
243.5	$\frac{15}{2}^- \rightarrow \frac{13}{2}^-$	41			0.66(10)	0.76(5)
258.7	$\frac{17}{2}^- \rightarrow \frac{15}{2}^-$	37			0.43(13)	0.81(11)
276.7	$\frac{19}{2}^- \rightarrow \frac{17}{2}^-$	22			0.61(23)	0.58(9)
287.0	$\frac{21}{2}^- \rightarrow \frac{19}{2}^-$	17				0.70(14)
289.6	$\frac{23}{2}^- \rightarrow \frac{21}{2}^-$	10				0.49(13)
257.0	$\frac{25}{2}^- \rightarrow \frac{23}{2}^-$	9			0.71(23)	0.59(11)
229.2	$\frac{27}{2}^- \rightarrow \frac{25}{2}^-$	3				0.85(18)
252.2	$\frac{29}{2}^- \rightarrow \frac{27}{2}^-$	4				
267.9	$\frac{31}{2}^- \rightarrow \frac{29}{2}^-$	3				0.65(18)
425.1	$\frac{13}{2}^- \rightarrow \frac{9}{2}^-$	90	1.25(9)	0.73(5)	0.93(7)	1.24(7)
502.2	$\frac{17}{2}^- \rightarrow \frac{13}{2}^-$	102	2.76(42)	0.47(7)	1.05(32)	1.20(14)

TABLE I. *(Continued).*

$E\gamma$(keV)[a]	$J_i^\pi \rightarrow J_f^\pi$[b]	I_γ[c]	λ[d]	$B(M1)/B(E2)$[e]	R_{DCO}	R_{ADO}
563.8	$\frac{21}{2}^- \rightarrow \frac{17}{2}^-$	74	4.35(44)	0.39(4)	0.96(20)	1.36(14)
546.6	$\frac{25}{2}^- \rightarrow \frac{21}{2}^-$	36	4.00(44)	0.50(5)	1.16(45)	1.36(9)
481.4	$\frac{29}{2}^- \rightarrow \frac{25}{2}^-$	4				1.15(16)
542.0	$\frac{33}{2}^- \rightarrow \frac{29}{2}^-$	4				1.30(45)
504.7	$\frac{21}{2}^- \rightarrow \frac{17}{2}^-$	46				
359.1	$\rightarrow \frac{27}{2}^-$	4				
Band 3						
562.1	$\frac{31}{2}^- \rightarrow \frac{27}{2}^-$	55				1.47(33)
504.5	$\frac{35}{2}^- \rightarrow \frac{31}{2}^-$	54			1.05(55)	1.49(48)
591.6	$\frac{39}{2}^- \rightarrow \frac{35}{2}^-$	15				1.15(32)
665.5	$\frac{43}{2}^- \rightarrow \frac{39}{2}^-$	8				1.33(25)
719.5	$\frac{47}{2}^- \rightarrow \frac{43}{2}^-$	5				1.31(45)
334.4	$\frac{27}{2}^- \rightarrow \frac{25}{2}^-$	208			0.73(9)	1.02(8)
202.6	$\frac{29}{2}^- \rightarrow \frac{27}{2}^-$	14				1.00(15)
359.4	$\frac{31}{2}^- \rightarrow \frac{29}{2}^-$	32			0.57(33)	0.76(34)
537.3	$\frac{29}{2}^- \rightarrow \frac{25}{2}^-$	108			0.93(12)	1.19(18)
509.1	$\frac{33}{2}^- \rightarrow \frac{29}{2}^-$	78			1.02(12)	1.29(13)
609.6	$\frac{37}{2}^- \rightarrow \frac{33}{2}^-$	51				1.33(22)
697.5	$\frac{41}{2}^- \rightarrow \frac{37}{2}^-$	20				1.54(75)
736.5	$\frac{45}{2}^- \rightarrow \frac{41}{2}^-$	7				
400.0	$\frac{25}{2}^- \rightarrow \frac{25}{2}^+$	12				
445.3	$\frac{21}{2}^- \rightarrow \frac{19}{2}$	33			0.92(32)	1.12(28)
715.0	$\frac{21}{2}^- \rightarrow \frac{21}{2}^+$	158			0.94(8)	1.27(4)
238.6	$\frac{25}{2}^- \rightarrow \frac{21}{2}^-$	82			1.13(13)	1.30(11)
755.2	$\frac{21}{2}^- \rightarrow \frac{19}{2}^+$	31			0.79(16)	0.74(15)
904.0	$\frac{17}{2}^- \rightarrow \frac{17}{2}^+$	39				
207.0	$\rightarrow \frac{17}{2}^-$	28				1.12(40)
223.7	$\frac{23}{2}^- \rightarrow$	31				
944.0	$\frac{17}{2}^- \rightarrow \frac{15}{2}^+$	18				0.94(20)
248.8	$\frac{21}{2}^- \rightarrow \frac{17}{2}^-$	54			1.16(23)	1.16(18)
182.0	$\frac{23}{2}^- \rightarrow \frac{21}{2}^-$	142			0.84(6)	0.87(4)
Structure 4						
401.7	$\frac{31}{2}^- \rightarrow \frac{27}{2}^-$	31				1.32(38)
436.0	$\frac{35}{2}^- \rightarrow \frac{31}{2}^-$	22				1.41(21)
548.7	$\frac{39}{2}^- \rightarrow \frac{35}{2}^-$	27				1.27(24)
377.8	$\frac{31}{2}^- \rightarrow \frac{27}{2}^-$	38				1.11(8)
460.0	$\frac{35}{2}^- \rightarrow \frac{31}{2}^-$	24				1.18(11)
369.8	$\frac{37}{2} \rightarrow \frac{35}{2}$	6				0.36(14)
550.7	$\frac{31}{2}^- \rightarrow \frac{27}{2}^-$	15				1.41(37)
294.1	$\frac{33}{2} \rightarrow \frac{31}{2}^-$	24			0.40(10)	0.59(4)
339.0	$\frac{35}{2} \rightarrow \frac{33}{2}$	16			0.40(13)	0.54(3)
306.0	$\frac{37}{2} \rightarrow \frac{35}{2}$	8			0.71(21)	0.61(9)
355.2	$\frac{39}{2} \rightarrow \frac{37}{2}$	4			0.54(32)	0.53(22)
224.0	$\frac{27}{2} \rightarrow \frac{25}{2}^-$	42			0.75(11)	0.90(13)
313.1	$\frac{29}{2}^- \rightarrow \frac{27}{2}$	17				

TABLE I. *(Continued).*

$E\gamma$(keV)[a]	$J_i^\pi \rightarrow J_f^\pi$[b]	I_γ[c]	λ[d]	$B(M1)/B(E2)$[e]	$R_{\rm DCO}$	$R_{\rm ADO}$
348.2	$\frac{31}{2}^- \rightarrow \frac{29}{2}^-$	5				
645.0	$\frac{37}{2} \rightarrow \frac{33}{2}$	9				
Band 4						
204.2	$\frac{7}{2}^- \rightarrow \frac{3}{2}^-$	42			1.14(12)	1.31(9)
296.0	$\frac{11}{2}^- \rightarrow \frac{7}{2}^-$	160			1.31(16)	1.44(10)
386.5	$\frac{15}{2}^- \rightarrow \frac{11}{2}^-$	167			0.92(12)	1.50(9)
463.0	$\frac{19}{2}^- \rightarrow \frac{15}{2}^-$	129			1.02(4)	1.22(6)
519.8	$\frac{23}{2}^- \rightarrow \frac{19}{2}^-$	49			1.08(13)	1.39(11)
523.8	$\frac{27}{2}^- \rightarrow \frac{23}{2}^-$	26			1.01(12)	1.19(16)
521.6	$\frac{31}{2}^- \rightarrow \frac{27}{2}^-$	9			0.92(48)	1.19(42)
115.6	$\frac{3}{2}^- \rightarrow \frac{3}{2}^-$	4				
164.9	$\frac{3}{2}^- \rightarrow \frac{5}{2}^-$	5				0.56(17)
178.8	$\frac{7}{2}^- \rightarrow \frac{5}{2}^-$	19			0.67(10)	0.61(7)
181.3	$\frac{3}{2}^- \rightarrow \frac{3}{2}^-$	18				
190.7	$\frac{3}{2}^- \rightarrow \frac{3}{2}^-$	26			0.96(16)	1.35(69)
490.0	$\frac{23}{2}^- \rightarrow \frac{19}{2}^-$	67			0.93(15)	1.25(11)
Band 5						
280.3	$\frac{9}{2}^- \rightarrow \frac{5}{2}^-$	320			1.06(5)	1.34(22)
388.6	$\frac{13}{2}^- \rightarrow \frac{9}{2}^-$	141			1.11(12)	1.22(4)
466.6	$\frac{17}{2}^- \rightarrow \frac{13}{2}^-$	121			1.15(7)	1.22(4)
530.6	$\frac{21}{2}^- \rightarrow \frac{17}{2}^-$	80			0.96(9)	1.21(8)
379.1	$\frac{25}{2}^- \rightarrow \frac{21}{2}^-$	76			1.10(9)	1.25(8)
411.6	$\frac{29}{2}^- \rightarrow \frac{25}{2}^-$	57			1.07(12)	1.21(7)
513.8	$\frac{33}{2}^- \rightarrow \frac{29}{2}^-$	40			1.05(34)	1.25(12)
610.5	$\frac{37}{2}^- \rightarrow \frac{33}{2}^-$	20				1.30(42)
700.6	$\frac{41}{2}^- \rightarrow \frac{37}{2}^-$	8				1.38(35)
194.5	$\frac{11}{2}^- \rightarrow \frac{9}{2}^-$	13			0.69(21)	0.70(13)
281.6	$\frac{21}{2}^- \rightarrow \frac{17}{2}^-$	13			0.94(13)	1.29(20)
628.1	$\frac{25}{2}^- \rightarrow \frac{21}{2}^-$	22			0.92(8)	1.17(12)
631.0	$\frac{25}{2}^- \rightarrow \frac{21}{2}^-$	18			0.95(22)	1.24(28)

[a]Uncertainties between 0.1 and 0.5 keV.
[b]See text for details about the spin and parity assignments.
[c]Uncertainties between 5 and 30%. Normalized to the 301.8-keV transition .
[d]Branching ratio: $T_\gamma(I \rightarrow I-2)/T_\gamma(I \rightarrow I-1)$, $T_\gamma(I \rightarrow I-2)$ and $T_\gamma(I \rightarrow I-1)$ are the relative γ-intensities of the $E2$ and $M1$ transitions depopulating the level I, respectively.
[e]Extracted from the branching ratios assuming $\delta^2 = 0$.

excitation energy transformed into the rotating frame [23]. The choice of the reference parameters is difficult in this transitional region, where the nuclei are relatively soft against changes in deformation as a function of rotational frequency and quasiparticle configuration. We have chosen a reference given by the Harris parametrization $J_0 = 23\hbar^2 \text{MeV}^{-1}$ and $J_1 = 40\hbar^4\,\text{MeV}^{-3}$, which give a nearly constant alignment in the $\nu i_{13/2}$ band of ^{187}Pt after the band crossing. The same parameters were used for all rotational bands. Examining Fig. 8, one can see that the rotational bands have apparent different slopes in the alignment curves before the band crossings, indicating likely the different deformation for each of the intrinsic state. Some interesting experimental results are given below.

In *band 1*, the two signatures show a rather large initial alignment of about $3.0\hbar$ and experience a pronounced backbending at $\hbar\omega \approx 0.29$ MeV. The $\alpha = +1/2$ branch shows a total alignment gain of about $8.0\hbar$ after the crossing, and this number is somewhat uncertain for the $\alpha = -1/2$ branch because the crossing is not yet completed at the last observed transition. One interesting feature here is that the band crossing frequency for the $\alpha = -1/2$ sequence is about 0.02 MeV lower than that for the $\alpha = +1/2$ one as estimated from Fig. 8(a), and the alignment gain after the band crossing is

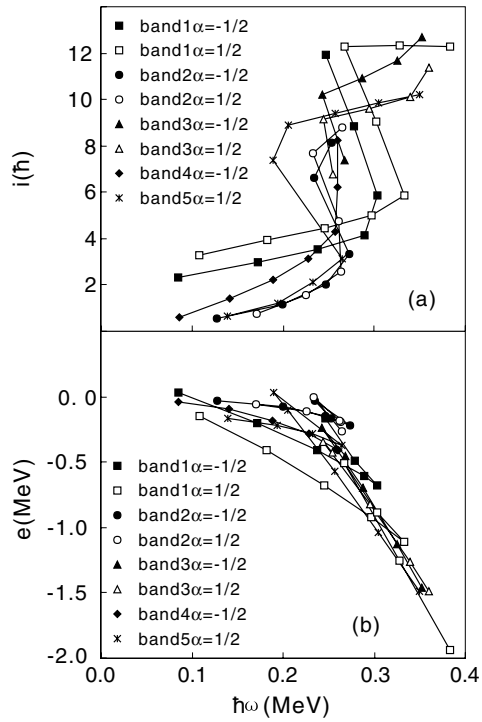

FIG. 8. Extracted alignment and Routhian energy for measured rotational bands in ^{187}Pt [panels (a) and (b), respectively]. The labels in the legends indicate the bands as they are labeled in Fig. 1. The Harris reference parameters are chosen to be $J_0 = 23\hbar^2$ MeV^{-1} and $J_1 = 40\hbar^4$ MeV^{-3}.

at least $1.0\hbar$ higher than that for the $\alpha = +1/2$ branch. This might be an indication of different shape driving effects of the quasiparticles in the two signatures of band 1. These two signatures have large energy splitting, and the energy splitting is increasing with frequency before the band crossing, with $\Delta e(\omega) = e(\omega, \alpha = -1/2) - e(\omega, \alpha = +1/2)$ reaching a maximum of about 250 keV at $\hbar\omega \approx 0.30$ MeV.

In *band 2*, the two signatures show almost identical behaviors up to the highest observed states. This band experiences a band crossing at $\hbar\omega = 0.25$ MeV and has no signature splitting over the whole frequency range covered in the present experiment. The total alignment gain is estimated to be of about $7.0\hbar$, although the highest-lying transitions needed to deduce this number are lacking.

In *band 3*, the two signature branches behave similarly, and no band crossing was observed below $\hbar\omega = 0.35$ MeV. The first points of the alignment curves deviate from the general trends, indicating likely that the band head is the $25/2^-$ state other than the $21/2^-$ state.

In *band 4*, there is an upbending at $\hbar\omega \approx 0.25$ MeV, and a complete crossing is not in sight at the last observed transition. The band crossing frequency and the slope of the alignment curve at low frequency are almost same as those of band 2.

Band 5 shows a very small initial alignment. This band experiences an acute backbending at $\hbar\omega = 0.22$ MeV with gain of $7.0\hbar$ in alignment.

The reason for the band crossings in ^{187}Pt is not obvious from Fig. 8. The high-j $\nu i_{13/2}$ and $\pi h_{9/2}$ orbits should be responsible for the alignment processes in this mass region. Although the $\nu i_{13/2}$ alignment is thought generally to be responsible for the first band crossing in many neutron-deficient Ir-Pt-Au nuclei, a low-frequency band crossing caused by the $\pi h_{9/2}$ alignment has been strongly suggested for several Ir-Pt-Au nuclei with neutron number of around 108 [8–15]. The nuclei in this transitional region are soft with respect to deformation, and the band crossing frequency is very sensitive to the deformation parameters of the intrinsic state in a given nucleus [8–10]. This makes it difficult to draw definite conclusion about the nature of the band crossing on the basis of the blocking argument and the systematics of the band crossings observed in neighboring nuclei. Detailed calculations of the influence of rotation on the nuclear shape should be undertaken for a proper understanding of the observed alignments in ^{187}Pt.

IV. THEORETICAL CALCULATIONS

To have a deeper understanding of the band structures in ^{187}Pt, we have performed CSM calculations by means of total Routhian surface (TRS) method [24] in the three-dimensional deformation β_2, β_4, and γ space. The nonaxial deformed Woods-Saxon (WS) potential [25] was employed. Both monopole and quadrupole pairings [26,27] were included. To avoid the spurious pairing phase transition encountered in the BCS approach, we used the approximate particle number projection named the Lipkin-Nogami pairing [28]. The pairing correlation is dependent on rotational frequency ($\hbar\omega$) and deformation. To include such dependence in the TRS calculations, we have done pairing-deformation-frequency self-consistent TRS calculations, i.e., for any given frequency and deformation, the pairing is self-consistently calculated by the HFB-like method [28]. At a given frequency, the deformation of a state is determined by minimizing the calculated TRS.

TRSs were calculated for the four lowest-lying configurations of each parity and signature combination. The variation of the shape parameters as a function of rotational frequency has been examined for these configurations. As examples of the calculations, Fig. 9 displays the TRSs of the lowest $(+, -1/2)$ and $(-, +1/2)$ configurations at $\hbar\omega = 0.10$ MeV (before the band crossing) and $\hbar\omega = 0.30$ MeV (after the band crossing). The TRSs are generally susceptive to the deformations and particularly soft with respect to the γ variations. At low rotational frequencies, there exists a minimum around $\beta_2 = 0.18 \sim 0.21$ and $\gamma = -30^\circ \sim +30^\circ$ for each of the parity and signature combination. This minimum is believed to be responsible for all the observed bands before the band crossings. The calculations indicate that the lowest-lying positive-parity configurations contain mainly the $11/2^+[615]$ and $9/2^+[624]$ Nilsson orbits originating from the $i_{13/2}$ subshell. In these configurations, the nucleus develops gradually a triaxial shape with $\gamma < 0^\circ$ as the rotational frequency increases. This is logical because the Fermi surface lies at the upper part of the $i_{13/2}$ subshell, which drives the deformation to negative γ values. The calculations also show that below the first band crossing the lowest $(+, +1/2)$ orbit of the $\nu i_{13/2}$ configuration drives the nucleus not only to

larger negative γ values but also to smaller values of β_2. In comparison, the $(+, -1/2)$ orbit has less shape driving tendency, especially in γ. It is therefore expected that the detailed alignment processes observed in the two signatures of the $\nu i_{13/2}$ configuration would be somewhat different, because the shapes are not exactly the same according to the calculations. The calculations predict that the lowest negative-parity states are the $\nu 3/2^-[512]$, $\nu 7/2^-[503]$, and $\nu 1/2^-[521]$ Nilsson configurations, which should be associated with the negative-parity bands observed experimentally. The shape parameters for these negative-parity configurations are rather different from those for the positive-parity ones. The negative-parity orbits influence the nuclear shape much less than the $\nu i_{13/2}$ orbits because of their smaller j values. The negative-parity orbits favor deformations with $\gamma > 0^\circ$ and large β_2 values although the potential surfaces are quite soft. Another striking feature predicted by the TRS calculations is the large and negative equilibrium hexadecapole deformation β_4 of about -0.04 for the configurations.

In the TRSs with both positive and negative parities, there exists another minimum at $\beta_2 \sim 0.19$ and $\gamma \sim -105^\circ$, i.e., the nucleus has a very triaxial shape close to the noncollective axis at $\gamma = -120^\circ$. These minimums would correspond to the structures with irregular level spacings observed experimentally.

The calculations predict that possible band crossings are due to the rotational alignment either of $i_{13/2}$ neutrons or of $h_{9/2}$ protons. The neutron and proton alignments can influence the nuclear deformation in different ways. As shown in Fig. 9, the $\nu i_{13/2}$ alignment results in an apparent deformation change toward negative γ values and smaller β_2 values. After the alignment, the three quasiparticle configuration with positive parity has a stiffer minimum located around at $\beta_2 \sim 0.155$ and $\gamma \sim -30^\circ$. However, the $\Omega = 1/2$ orbit of the $h_{9/2}$ subshell is close to the proton Fermi surface, and therefore the alignment of the $\pi h_{9/2}$ pair drives the deformation toward to positive γ values. The potential surface involving the aligned $h_{9/2}$ protons is very soft both in the γ and β_2 directions.

To get aid in the understanding of the experimentally observed band crossings, CSM calculations were performed with $\beta_2 = 0.155$ and 0.20, which represent the quadrupole deformations predicted by the TRS calculations for the configurations involving the aligned $i_{13/2}$ neutrons and $h_{9/2}$ protons, respectively. Due to the predicted very γ softness, we varied the γ values from -30° to $+30^\circ$. With the different deformations, we plotted quasi-neutron and quasiproton Routhians as shown in Figs. 10 and 11. The calculations show that the band crossing frequencies are strongly dependent on the deformations. It is clear that small β_2 and negative γ values lower the $\nu i_{13/2}$ crossing frequencies, and the negative γ values shift the $\pi h_{9/2}$ alignment to high frequencies. However, the frequency of the $\pi h_{9/2}$ alignment gradually decreases while increasing the γ value. The calculations show that a larger quadrupole deformation can induce a delayed $\nu i_{13/2}$ alignment but an earlier $\pi h_{9/2}$ alignment. We also did the configuration-constraint calculations [29] for the negative-parity configurations, and found that the $\nu 1/2^-[521]$ configuration has a larger quadrupole deformation than those of the other negative configurations.

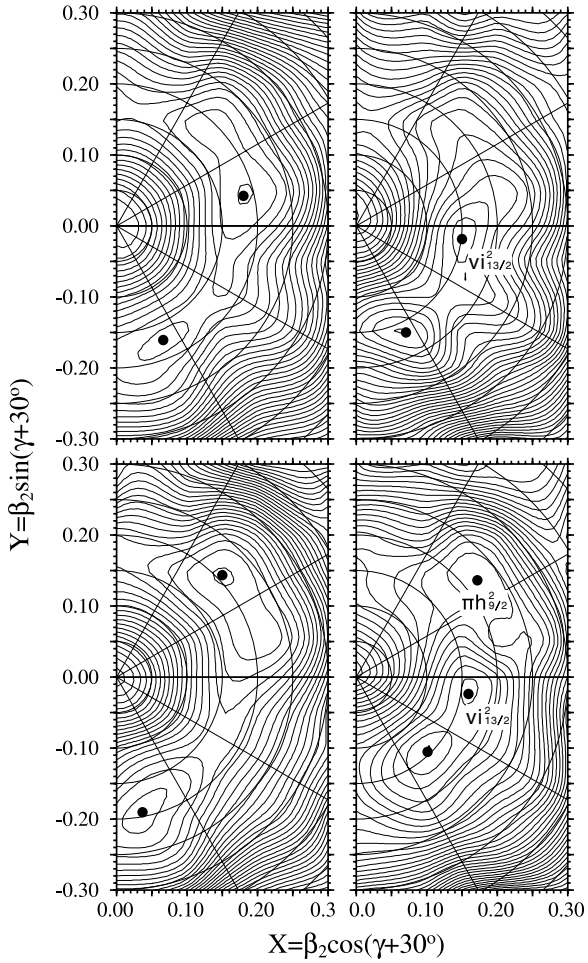

FIG. 9. Calculated total Routhian surfaces for the lowest $(\pi, \alpha) = (+, -1/2)$ (top panels) and $(-, +1/2)$ (bottom panels) configurations at $\hbar\omega = 0.10$ MeV (left panels) and $\hbar\omega = 0.30$ MeV (right panels).

V. DISCUSSION

A. Band 1, based on the $\nu i_{13/2}$ configuration

The $\nu i_{13/2}$ configuration has been assigned to band 1 [19,20]. In the heavier odd-A Pt isotopes [19,30,31], a decoupled band associated with the $\nu i_{13/2}$ configuration has been observed systematically, and it displays level spacings very similar to those of the ground-state band in the adjacent even-even Pt nucleus. Band 1 resembles closely the $\nu i_{13/2}$ bands observed in the heavier odd-A Pt nuclei [19,30,31]. One of the interesting findings in the present work is the observation of the unfavored signature branch up to high spin, whereas in the heavier odd-A Pt nuclei only was a short sequence observed [19,30,31]. As shown in Fig. 8, this band has an initial alignment of about $3.0\hbar$. The alignments were deduced by assuming a band head K value of 5.5, because the theoretical calculations suggested a main component of the $11/2^+[615]$ orbit in the configuration of band 1. The $11/2^+$ band head was located 29 keV below the $13/2^+$ state in ^{187}Pt. However, the $11/2^+$ band head lies 49, 24, and 11 keV above the $13/2^+$ level in ^{193}Pt, ^{191}Pt, and ^{189}Pt, respectively [30]. The lowering of the band head energy with decreasing mass number would interpret the observation of the long unfavored signature

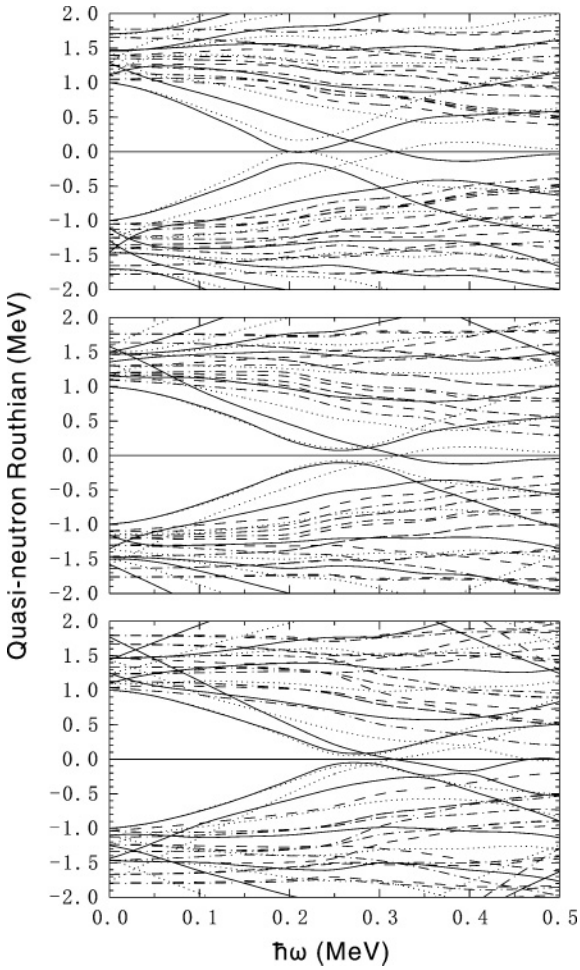

FIG. 10. Calculated quasineutron Routhians as a function of rotational frequency ($\hbar\omega$) in ^{187}Pt. In the calculations, we set $\beta_2 = 0.155$ and $\beta_4 = -0.04$. The γ deformations were fixed at -15°, 0°, and 15° for the top, middle, and bottom panels, respectively. The parity and signature (π, α) of the Routhians are represented as follows: $(+, +1/2)$ solid lines, $(+, -1/2)$ dotted lines, $(-, +1/2)$ dash-dotted lines, and $(-, -1/2)$ dashed lines. The lowest neutron Routhians with $\alpha = +1/2$ and $-1/2$ are the $i_{13/2}$ orbits.

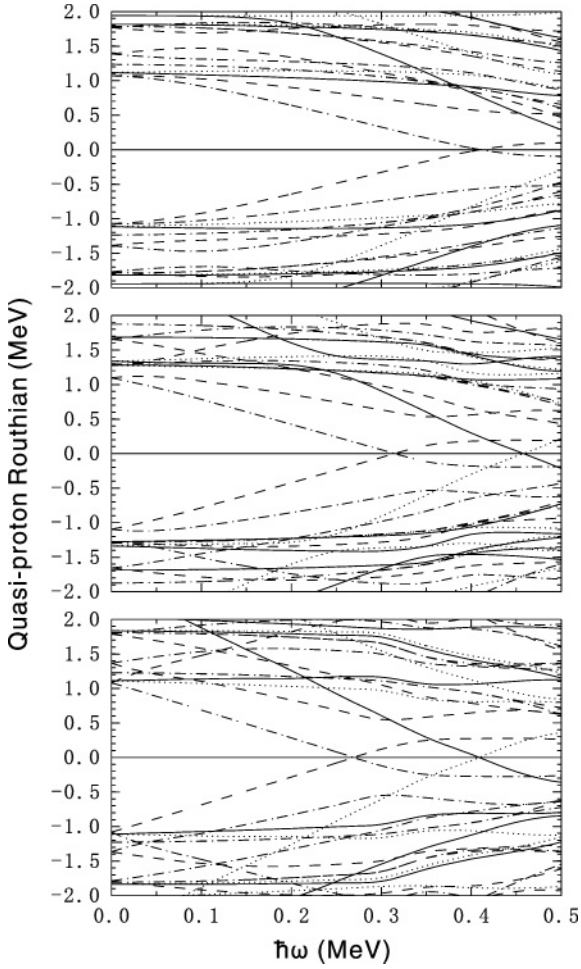

FIG. 11. Calculated quasiproton Routhians as a function of rotational frequency ($\hbar\omega$) in ^{187}Pt. In the calculations, we set $\beta_2 = 0.20$ and $\beta_4 = -0.04$. The γ deformations were fixed at -15°, 0°, and 15° for the top, middle, and bottom panels, respectively. The parity and signature (π, α) of the Routhians are represented as follows: $(+, +1/2)$ solid lines, $(+, -1/2)$ dotted lines, $(-, +1/2)$ dash-dotted lines, and $(-, -1/2)$ dashed lines. The lowest proton Routhians with $\alpha = +1/2$ and $-1/2$ are the $h_{9/2}$ orbits.

sequence in ^{187}Pt. The continuously lowering of the energy of the unfavored levels should be resulted from two factors [30]. One is the location of the Fermi surface deeper within the $\nu i_{13/2}$ subshell with decreasing mass number. The other is the increase of the quadrupole deformation and the change of γ deformation toward a prolate shape as the mass number decreases, therefore favoring strong coupling over decoupling. The low-spin structure of the $\nu i_{13/2}$ bands in the heavier odd-A Pt nuclei has been well described by the asymmetric rotor model [30].

The calculations predict that the first band crossing for the $\nu i_{13/2}$ band should result from the alignment of a pair of $i_{13/2}$ neutrons (BC and AD crossings) due to the appreciable negative γ deformation. For the favored signature branch, the band crossing takes place at $\hbar\omega = 0.30$ MeV, and the associated gain in alignment is about $8.0\hbar$, as deduced from Fig. 8. The gain in alignment is about the same as that for the alignment of a BC neutron pair in the neighboring odd-A nuclei [31–34], whereas the band crossing frequency is much higher than the BC crossing frequencies. The decoupled $\nu i_{13/2}$ band in ^{191}Pt experiences the BC crossing at $\hbar\omega = 0.29$ MeV [31], and this crossing occurs at $\hbar\omega \approx 0.27$ MeV in the odd-A Hg nuclei [32–34]. The delay of the BC crossing in the Pt nuclei may be due to the different shapes of the crossing bands. According to the TRS calculations for ^{187}Pt, the nuclear shape of band 1 changes greatly both in β_2 and γ values after the band crossing. The BC crossing in ^{191}Pt corresponds to a shape change from $\gamma \sim -45^\circ$ triaxial to $\gamma \sim -60^\circ$ oblate, but β_2 remaining unchanged [31], whereas the crossing bands in the odd-A Hg isotopes have the same oblate shape [32–34]. For the unfavored signature branch of the $\nu i_{13/2}$ band in ^{187}Pt, we could not deduce accurately the band crossing frequency and the gain in alignment because a complete alignment process is not in sight. But there exist apparent differences between the alignment processes for the two signature partners. From Fig. 8, we can estimate that the band crossing frequency for

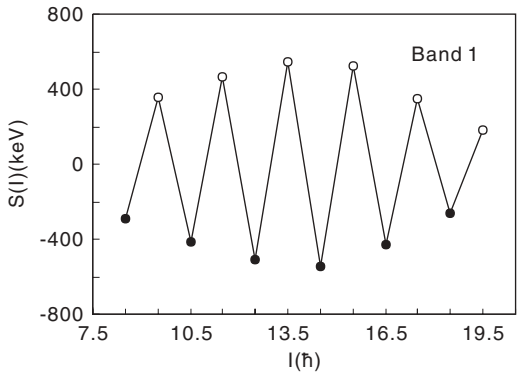

FIG. 12. Signature splitting $S(I)$ as a function of spin I for the $\nu i_{13/2}$ band in ^{187}Pt. The filled and open symboles correspond to the favored and unfavored signatures, respectively.

the $\alpha = -1/2$ sequence is about 0.02 MeV lower than that for the $\alpha = +1/2$ one, and the alignment gain associated with the band crossing is at least $1.0\hbar$ higher than that for the $\alpha = +1/2$ branch. These differences might be caused by the different nuclear shapes of the two signatures as pointed out in the previous section. The band crossing frequencies for the $\nu i_{13/2}$ band can be well reproduced theoretically by assuming a appropriate deformation, for example, $\beta_2 \sim 0.155$ and $\gamma \sim -30^\circ$. We should mention here that the close-lying 10^+ states below the yrast 12^+ level were observed in ^{188,190,192}Pt, and the reduced transition probabilities between the concerned states were measured experimentally [19,35]. It was strongly suggested that the alignments of the $h_{11/2}$ protons and the $i_{13/2}$ neutrons at nearly degenerate frequencies are both important in interpreting the observed structure in these even-even Pt nuclei [19,35]. However, the calculations predict that the $h_{11/2}$ and $h_{9/2}$ proton alignments always occur at high frequencies for appreciable negative γ deformations.

The $\nu i_{13/2}$ band displays very large signature splitting in the whole spin region observed experimentally. The signature splitting Δe is defined as the difference in energies at a given rotational frequency for the pair of signature partners. Figure 12 presents a plot of the signature splitting for the $\nu i_{13/2}$ band, defined as [36]

$$S(I) = [E(I) - E(I-1)] - \tfrac{1}{2}[E(I+1) - E(I) + E(I-1) - E(I-2)]. \quad (3)$$

Here $E(I)$ is the level energy of state I; $S(I)$ is directly proportional to the signature splitting Δe, but magnified by approximately a factor of 2. As shown in Fig. 12, there is a significant energy splitting between the two signatures at low frequencies, and after the $i_{13/2}$ neutron alignment the splitting is still kept with the amplitude almost unchanged. Signature splitting of the energies is considered generally as a consequence of the mixing of the $\Omega = 1/2$ orbits into the wave functions due to the Coriolis interaction. Because the neutron Fermi level lies high in the $i_{13/2}$ subshell in ^{187}Pt with a neutron number of 109, the mixing of the $\Omega = 1/2$ components into the wave functions should be very small for an axially symmetric nuclear shape. To explain the large signature splitting in the $\nu i_{13/2}$ band, a mechanism leading to enhanced mixing with an $\Omega = 1/2$ orbit is needed. In the lighter odd-A Pt nuclei [9,37,38], large signature splitting was also observed in the $\nu i_{13/2}$ bands. It was proposed that it is the negative values of γ and β_4 that cause this phenomenon [37,38]. The same explanation could be applied to ^{187}Pt. The TRS calculations indicate that the $\nu i_{13/2}$ configurations have large and negative equilibrium hexadecapole deformation of about -0.04. A large negative value of β_4 can bunch the single-particle levels and brings the low-Ω orbits closer to the Fermi surface. The triaxiality can induce a similar effect. As shown in Fig. 10, the large signature splitting in the $\nu i_{13/2}$ band was quite well reproduced by the large negative γ and β_4 values.

Several structures with irregular level spacings were observed to feed the $\nu i_{13/2}$ band. Interesting feature is that structures 1 and 2 decay only to the unfavored levels of the $\nu i_{13/2}$ band, whereas structure 3 is connected solely with the favored levels. These structures should have close relationships with the $\nu i_{13/2}$ configuration and might be associated with the predicted potential minimums with γ values close to -120°.

B. Band 2, based on the $\nu 7/2^-[503]$ configuration

The band head spin and parity of band 2 were assigned to be $7/2^-$ [20]. This strongly coupled band experiences a sharp backbending at $\hbar\omega = 0.25$ MeV with gain of $7.0\hbar$ in alignment (see Fig. 8). The TRSs of the negative-parity configurations shown in Fig. 9 correspond to this band, as it is the negative-parity yrast band at low spins. The calculated potential surfaces for this band are very soft with respect to the β and γ variations at low frequencies. For a near prolate deformation in this mass region, the $\nu 7/2^-[503]$ and $\nu 7/2^-[514]$ Nilsson orbits lie close to the Fermi surface, and there may be some mixing between them. The observed low initial alignment and the absence of any signature splitting are consistent with the assignment of either $\nu 7/2^-[503]$ or $\nu 7/2^-[514]$ Nilsson configuration to band 2.

The $B(M1)/B(E2)$ ratios for a coupled band have been proven to be quite useful in characterizing the specific intrinsic orbit and the quasiparticles associated with band crossing. Information concerning the quasiparticle makeup of band 2 can be obtained by comparing theoretical $B(M1)/B(E2)$ values with experimental ones. The experimental $B(M1)/B(E2)$ ratios have been deduced according to the Eq. (2). The experimental data are shown in Fig. 13 together with theoretical estimates obtained from a semiclassical formulas [39,40]

$$\frac{B(M1; I \to I-1)}{B(E2; I \to I-2)} = \frac{12}{5Q_0^2\cos^2(\gamma+30^\circ)} \times \left[1 - \frac{K^2}{(I-1/2)^2}\right]^{-2} \frac{K^2}{I^2} \times \{(g_{K1} - g_R)[(I^2-K^2)^{1/2} - i_1] - (g_{K2} - g_R)i_2\}^2 \left(\frac{\mu_N^2}{e^2b^2}\right). \quad (4)$$

This expression takes into account the effect of triaxiality γ on $E2$ transition rate. The suffixes 1 and 2 refer to the strongly coupled and decoupled quasiparticles, respectively.

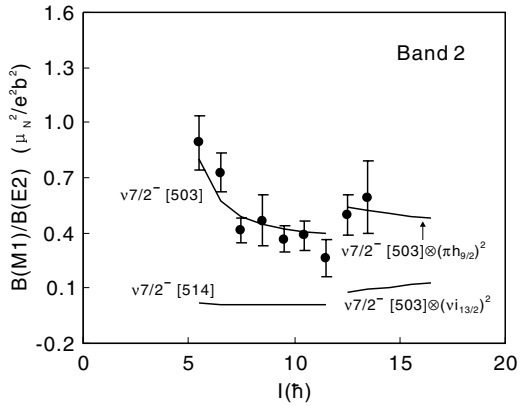

FIG. 13. Experimental $B(M1)/B(E2)$ ratios as a function of initial spin I for the $7/2^-[503]$ band and theoretical predictions assuming $\gamma = 0^\circ$ for the $7/2^-[503]$ and $7/2^-[514]$ configurations as described in the text. The theoretical results for the $\nu i_{13/2}$ and $\pi h_{9/2}$ alignments are also presented.

In the calculations, the quasiparticle gyromagnetic g_K-g_R factors were taken from Refs. [38,41]. The alignment of the strongly coupled particle was set to $i_1 = 0.5\hbar$, and a value $i_2 = 7.0\hbar$ as deduced from experiment was used for the decoupled quasiparticle pair. The nominal band head K value of 3.5 was used. The quadrupole moment was set to $Q_0 = 5.7$ eb, which corresponds to the quadrupole deformation of the neighboring even-even nucleus ^{186}Os [42]. We used $\gamma = 0^\circ$ in the calculations. The experimentally extracted $B(M1)/B(E2)$ ratios before band crossing are compared with the calculated results by assuming the $\nu 7/2^-[503]$ and $\nu 7/2^-[514]$ Nilsson configurations, respectively. Rotational bands based on these two Nilsson orbits have very different gyromagnetic factors, resulting from the $l + s(f_{7/2})$ and $l - s(h_{9/2})$ spin-orbit coupling. As clearly shown in Fig. 13, the experimental values are well reproduced by the configuration of $\nu 7/2^-[503](f_{7/2})$, whereas the calculated values associated with the $\nu 7/2^-[514](h_{9/2})$ configuration are far below the experimental observations. Therefore, we propose that band 2 is based on the rather pure $\nu 7/2^-[503](f_{7/2})$ configuration. The negative-parity configurations have soft potential surfaces with respect to γ deformation at low frequencies. We examined the effects of γ variations on the theoretical ratios and found that the $\nu 7/2^-[503]$ configuration is strongly preferred in the γ interval from -20° to $+20^\circ$.

The experimental $B(M1)/B(E2)$ ratios for the $\nu 7/2^-[503]$ band show a pronounced increase of a factor of 2 in the band crossing region. In the mass region of the present interest, the $i_{13/2}$ neutrons and $h_{9/2}$ protons should be responsible for the band crossing. Due to the opposite signs of the proton versus neutron g factors, the $h_{9/2}$ proton alignment in the $\nu 7/2^-[503]$ band should lead to an increase in the $B(M1)$ value, whereas the $i_{13/2}$ neutron alignment has the opposite effect. Assuming the same deformation before and after the band crossing, the theoretical $B(M1)/B(E2)$ ratios associated with the neutron and proton alignments are shown in Fig. 13. As expected the two alignments result in opposite trends in the $B(M1)/B(E2)$ values after the crossing. We have to point out that the deformation may be changed by the alignment. Consequently, this changing deformation affects the $B(E2)$ value. Therefore, the difference in the magnitude of change in $B(M1)/B(E2)$ values after the band crossing should be carefully examined by taking into account of the changing deformation. Because the Fermi surface lies in the upper part of the $\nu i_{13/2}$ subshell for a near prolate shaped nucleus with a neutron number of 109, the alignment of the $\nu i_{13/2}$ pair drives the deformation to negative γ and smaller β_2 values as demonstrated by the TRS calculations. The proton Fermi surface is close to the $\Omega = 1/2$ level of the $h_{9/2}$ subshell, and thus the alignment of the $\pi h_{9/2}$ pair triggers a deformation change to positive γ value. Regarding the proton alignment, the associated γ shift to positive direction causes an increase of the $B(M1)/B(E2)$ values. For the alternative neutron alignment, a small change of the quadrupole moment affects the calculated ratios only slightly, and a large negative γ value decreases the $B(M1)/B(E2)$ ratios. The general trends shown in Fig. 13 could not be changed if we take into account of the deformation changes associated with the neutron and proton alignments. Therefore, the experimentally observed increase in the $B(M1)/B(E2)$ ratios strongly suggest that the band crossing is due to the $h_{9/2}$ proton alignment. To get an definite conclusion about the nature of the band crossing, the $\nu 7/2^-[503]$ band should be extended to high-spin states, and the $B(E2)$ values after the band crossing should be measured experimentally.

The nucleus ^{187}Pt has a neutron number of 109, and there exist a large gap in the single-particle levels at $N = 108$ for a near prolate deformation. This gap moves the Fermi surface far away from the low-Ω orbits of the $i_{13/2}$ subshell, which could lead to a significant delay for the neutron AB crossing. The CSM calculations display that the $i_{13/2}$ neutron alignment occurs at high frequencies if we use the deformation parameters of $\gamma > 0^\circ$ and $\beta_2 \sim 0.16$. However, the $h_{9/2}$ protons align at quite low frequency by assuming positive γ values, as shown in Fig. 11. The predicted potential minimum for the $\nu 7/2^-[503]$ configuration is located at $\gamma > 0^\circ$ as indicated in Fig. 9 although the potential surface is quite γ soft. The CSM calculations strongly support the low-frequency $h_{9/2}$ proton alignment in the $\nu 7/2^-[503]$ band. However, it is worth noting that the pronounced energy gap at $N = 108$ is associated with a prolate shape, which does not appear at deformations with $\gamma \leqslant -15^\circ$. If the negative-parity bands have an appreciable negative γ deformation, the neutron AB alignment can also occur at low frequency.

C. Band 3, based on the $\nu i_{13/2}^2 \nu j(p_{3/2}$ or $f_{5/2})$ configuration

Semidecoupled bands built on the 5^- state have been generally observed in the even-even Pt and Hg nuclei [19,35,43]. The intrinsic structure of the 5^- state in the even-even nuclei was proposed to be dominated by the two quasiparticle configuration $\nu i_{13/2} \nu j$ (νj originating from $p_{3/2}$ or $f_{5/2}$), the high-j quasiparticle being decoupled from the rotational core and the low-j one being strongly coupled to the core [44,45]. Rotational band built on the $21/2^-$ state, which was formed by coupling an additional $i_{13/2}$ quasineutron to the 5^- state in the neighboring even-even nucleus, has been also systematically

observed in the odd-A Pt and Hg nuclei [19,30–34]. The structure of band 3 follows closely the systematics of the rotational bands built on the $21/2^-$ state in the heavier odd-A Pt nuclei [19,30,31], and we therefore propose that band 3 is associated with the configuration of $\nu i_{13/2}^2 \nu j$. Although these negative-parity bands in the Pt and Hg nuclei show marked similarities, there exist distinctive differences between the Pt and Hg nuclei. One is that the $9^- \rightarrow 7^-(29/2^- \rightarrow 25/2^-)$ level spacings in the Pt nuclei are much larger than those observed in the Hg nuclei, which can be well explained by the particle-rotor model assuming a triaxial nuclear shape for the Pt nuclei [45]. The other one is that the excitation energies of the $5^-(21/2^-)$ states in the Pt nuclei are several hundred keV lower than those in the Hg nuclei, which was reproduced theoretically by including a large contribution of the proton excitation of $\pi h_{11/2} \pi j$ (πj being $s_{1/2}$ or $d_{3/2}$) in the $5^-(21/2^-)$ states in the Pt isotopes [45].

As shown in Fig. 8, band 3 has large aligned angular momenta of about $10.0\hbar$ and $11.0\hbar$ for the two signatures, respectively. The alignment was deduced by assuming a band head K value of 4.5; the alignment in such high-spin levels is expected to be less influenced by the uncertainty of the K value. The absence of any band crossing below $\hbar\omega = 0.35$ MeV likely suggests that band 3 involves two neutrons occupying the $i_{13/2}$ orbits and has negative γ deformation. Because the Fermi surface lies in the upper part of the $\nu i_{13/2}$ subshell, the $\nu i_{13/2}^2 \nu j$ configuration would favor negative γ deformation. As shown in Fig. 11, the negative γ deformation shifts the band crossing caused by the proton alignment to very high frequency. The occupation of two neutrons in the $\nu i_{13/2}$ subshell would inhibit the $\nu i_{13/2}$ alignments (AB, BC, and AD) from occurring at the expected frequencies. If the band head is the $21/2^-$ state, it is expected that the $27/2^- \rightarrow 23/2^- E2$ transition should be strong enough to be observed experimentally. However, we have not gotten any evidence for the existence of this transition within the detection sensitivity in the present work. Furthermore, the decay patterns of the $23/2^-$ and $25/2^-$ states are quite complicated and the first points in the alignments shown in Fig. 8 are well below the averaged values. It seems therefore reasonable to propose that the band head of band 3 in ^{187}Pt is the $25/2^-$ state other than the $21/2^-$ state.

D. Band 4, based on the $\nu 3/2^-[512]$ configuration

Band 4 is built on the ground state, which was suggested to be the $\nu 3/2^-[512]$ Nilsson configuration [3–5]. If the $\nu 3/2^-[512]$ Nilsson configuration has an axial symmetric deformation, a coupled band would be observed experimentally. The isotope shift and hyperfine structure measurements strongly suggested a triaxial shape for the ground state of ^{187}Pt [3–5], which was supported by the TRS calculations. The theoretical calculations show that the triaxiality can induce a large signature splitting in energy for the two signature branches associated with the $\nu 3/2^-[512]$ configuration, and this might explain the nonobservation of the unfavored level sequence in the present work. As shown in Fig. 8, the alignment of band 4 starts an upbending at $\hbar\omega \approx 0.25$ MeV. The alignment process of band 4 is closely similar with that of the $\nu 7/2^-[503]$ band; the slope of the alignment before the band crossing and the band crossing frequency are almost same as those of the $\nu 7/2^-[503]$ band. Therefore, the band crossing in band 4 is likely caused by the $h_{9/2}$ proton alignment. The $7/2^-$ and $11/2^-$ levels of band 4 decay to the $5/2^-$ and $9/2^-$ levels of band 5, indicating that there exists interaction between these two bands at low spins.

E. Band 5, based on the $\nu 1/2^-[521]$ configuration

Band 5 has a decoupled structure, suggesting that the configuration includes a neutron from an $\Omega = 1/2$ orbit. Candidate orbits are $\nu 1/2^-[521]$ and $\nu 1/2^-[510]$, which lie near the Fermi surface. The $\nu 1/2^-[521]$ state was determined to be the ground state for ^{179,181,183} Pt [37,38,46], and the decoupled $\nu 1/2^-[521]$ band was systematically observed in the lighter odd-A Pt nuclei. The $\nu 1/2^-[510]$ state was assigned as the ground state of the lighter isotones of ^{187}Pt, and the ground-state bands were also identified experimentally [41,47]. We therefore propose that band 5 should be associated with either the $\nu 1/2^-[521]$ configuration or the $\nu 1/2^-[510]$ configuration. The level energies of a decoupled band can be described by the formulas

$$E(I) = \frac{\hbar^2}{2\Im}[I(I+1) + a(-1)^{I+1/2}(I+1/2)]. \quad (5)$$

The decoupling parameter a is very characteristic for the configuration involved. We deduced the decoupling parameter a from the excitation energies of the levels with spins of 5/2, 9/2, and 13/2 for the concerned decoupled bands. Band 5 has a negative a value of -2.4, and this can be compared with $a = -1.2$ and 0.7 for the $\nu 1/2^-[521]$ bands in ^{183}Pt and ^{185}Pt [9,10,37], respectively. However, the decoupling parameter a has positive valves of 0.8 and 0.5 for the $\nu 1/2^-[510]$ bands in the isotones ^{185}Os and ^{183}W [41,47]. Generally, the $\nu 1/2^-[521]$ band in the odd-A Pt nuclei displays large signature splitting [37,38,46], whereas the $\nu 1/2^-[510]$ band in the isotones of ^{187}Pt shows very small signature splitting, and the unfavored signature branch was also observed experimentally [41,47]. Comparing the level spacings of band 5 with those of the $\nu 1/2^-[521]$ and $\nu 1/2^-[510]$ bands in the neighboring nuclei, we can find that band 5 follows very well the trends of the $\nu 1/2^-[521]$ bands in the lighter odd-A Pt nuclei [37,38,46]. Therefore, band 5 might be based on the $\nu 1/2^-[521]$ Nilsson orbit. In the previous work [16], the $\nu 5/2^-[532]$ configuration with an oblate shape was very tentatively assigned to the 25.0-keV state.

Band 5 has a very small initial alignment, in agreement with what is expected for an aligned neutron state occupying the $1/2^-[521]$ orbit. As shown in Fig. 8, the band crossing takes place at $\hbar\omega = 0.22$ MeV, where the gain in the alignment is about $7.0\hbar$. In the lighter odd-A Pt nuclei [37,38,46], the $1/2^-[521]$ band experiences a band crossing at $\hbar\omega \approx 0.23$ MeV, which was attributed to the alignment of a pair of neutrons in the $i_{13/2}$ subshell. Based on the systematics of band crossings in the $\nu 1/2^-[521]$ bands, it then seems to be a natural proposal that the band crossing in band 5 is caused by

the neutron AB alignment. However, as pointed out previously the large gap in the single-particle levels at $N = 108$ should lead to a significant delay for the neutron AB crossing in ^{187}Pt, which was supported by the CSM calculations. It is very possible that the band crossing of band 5 has a same nature as the $\nu 7/2^-[503]$ band, being caused by the alignment of $h_{9/2}$ protons. The calculations indicate that the $\nu 1/2^-[521]$ configuration has a larger quadrupole deformation than the other negative-parity configurations. The $\nu 1/2^-[521]$ orbit has a negative slope in the Nilsson diagrams and thus drives the nucleus toward larger quadrupole deformation. Because the proton Fermi level, λ_π, is below the low-$\Omega h_{9/2}$ proton orbits, an increased deformation corresponds to a decreased quasiproton energy, E_π, for the $h_{9/2}$ quasiproton:

$$E_\pi = \sqrt{\Delta^2 + (\varepsilon_\pi - \lambda_\pi)^2}, \tag{6}$$

resulting in a earlier band crossing than that in the $\nu 7/2^-[503]$ band.

VI. SUMMARY

The transitional nucleus ^{187}Pt has been produced in the bombardment of the ^{173}Yb target with the ^{18}O projectiles. The previously known bands based on the $\nu i_{13/2}$, $\nu 7/2^-[503]$, and $\nu i_{13/2}^2 \nu j$ configurations have been extended significantly to high-spin states, and new rotational bands associated with the $\nu 3/2^-[512]$ and $\nu 1/2^-[521]$ Nilsson orbits have been identified. The possible quasiparticle configurations of these bands have been proposed based on the measured in-band $B(M1)/B(E2)$ ratios and the existing knowledge of band structures in the neighboring nuclei. The TRS calculations show that the nucleus ^{187}Pt is very soft with respect to γ and β_2 deformations. The $\nu i_{13/2}$ band has an appreciable negative γ deformation, and the band crossing was attributed to the alignment of a pair of $i_{13/2}$ neutrons (BC and AD crossings). There is a large energy splitting between the two signatures of the $\nu i_{13/2}$ band, and the large signature splitting was quite well reproduced by the large negative γ and β_4 values predicted by the TRS calculations. The negative-parity $\nu 7/2^-[503]$, $\nu 3/2^-[512]$, and $\nu 1/2^-[521]$ bands show band crossings at low frequencies. The experimentally measured $B(M1; I \to I-1)/B(E2; I \to I-2)$ ratios strongly support the low-frequency $h_{9/2}$ proton alignment in the $\nu 7/2^-[503]$ band. The TRS calculations show that the negative-parity configurations tend to have a near prolate shape with small positive γ values. Due to the existence of a large gap in the single-particle levels at $N = 108$ for a near prolate deformation, the $i_{13/2}$ neutron alignment might be shifted significantly to high frequencies in the negative-parity bands. By assuming positive γ deformations, the low-frequency $h_{9/2}$ proton alignment can be well reproduced by the CSM calculations.

ACKNOWLEDGMENTS

The research was performed with JAEA Common Use Facility Program. The authors thank the staff at the JAEA tandem accelerator for providing the ^{18}O beam. This work was supported by the National Natural Sciences Foundation of China (grant 10505025 and 10475097) and the Chinese Academy of Sciences.

[1] J. L. Wood, K. Heyde, W. Nazarewicz, M. Huyse, and P. Van Duppen, Phys. Rep. **215**, 101 (1992).
[2] D. T. Joss, J. Simpson, D. E. Appelbe, C. J. Barton, D. D. Warner, K. Lagergren, B. Cederwall, B. Hadinia, S. Eeckhaudt, T. Grahn, P. T. Greenlees, P. M. Jones, R. Julin, S. Juutinen, H. Kettunen, M. Leino, A. P. Leppänen, P. Nieminen, J. Pakarinen, J. Perkowski, P. Rahkila, C. Scholey, J. Uusitalo, K. Van de Vel, R. D. Page, E. S. Paul, D. R. Wiseman, and M. A. Riley, Phys. Rev. C **74**, 014302 (2006).
[3] H. T. Duong, J. Pinard, S. Liberman, G. Savard, J. K. P. Lee, J. E. Crawford, G. Thekkadath, F. Le Blanc, P. Kilcher, J. Obert, J. Oms, J. C. Putaux, B. Roussière, J. Sauvage, and ISOCELE Collaboration, Phys. Lett. **B217**, 401 (1989).
[4] J. K. P. Lee, G. Savard, J. E. Crawford, G. Thekkadath, H. T. Duong, J. Pinard, S. Liberman, F. Le Blanc, P. Kilcher, J. Obert, J. Oms, J. C. Putaux, B. Roussiere, and J. Sauvage, Phys. Rev. C **38**, 2985 (1988).
[5] A. E. Stuchbery, S. S. Anderssen, A. P. Byrne, P. M. Davidson, G. D. Dracoulis, and G. J. Lane, Phys. Rev. Lett. **76**, 2246 (1996).
[6] G. D. Dracoulis, A. E. Stuchbery, A. P. Byrne, A. R. Poletti, S. J. Poletti, J. Gerl, and R. A. Bark, J. Phys. G **12**, L97 (1986).
[7] G. Hebbinghaus, W. Gast, A. Kramer-Flecken, R. M. Lieder, J. Skalski, and W. Urban, Z. Phys. A **328**, 387 (1987).
[8] M. P. Carpenter, C. R. Bingham, L. H. Courtney, V. P. Janzen, A. J. Larabee, Z. M. Liu, L. L. Riedinger, W. Schmitz, R. Bengtsson, T. Bengtsson, W. Nazarewicz, J. Y. Zhang, J. K. Johansson, D. G. Popescu, J. C. Waddington, C. Baktash, M. L. Halbert, N. R. Johnson, I. Y. Lee, Y. S. Schutz, J. Nyberg, A. Johnson, R. Wyss, J. Dubuc, G. Kajrys, S. Monaro, S. Pilotte, K. Honkanen, D. G. Sarantites, and D. R. Haenni, Nucl. Phys. **A513**, 125 (1990).
[9] S. Pilotte, G. Kajrys, S. Monaro, M. P. Carpenter, V. P. Janzen, L. L. Riedinger, J. K. Johansson, D. G. Popescu, D. D. Rajnauth, and J. C. Waddington, Phys. Rev. C **40**, 610 (1989).
[10] V. P. Janzen, M. P. Carpenter, L. L. Riedinger, W. Schmitz, S. Pilotte, S. Monaro, D. D. Rajnauth, J. K. Johansson, D. G. Popescu, J. C. Waddington, Y. S. Chen, F. Donau, and P. B. Semmes, Phys. Rev. Lett. **61**, 2073 (1988).
[11] J. K. Johansson, D. G. Popescu, D. D. Rajnauth, J. C. Waddington, M. P. Carpenter, L. H. Courtney, V. P. Janzen, A. J. Larabee, Z. M. Liu, and L. L. Riedinger, Phys. Rev. C **40**, 132 (1989).
[12] D. L. Balabanski, W. Gast, G. Hebbinghaus, A. Kramer-Flecken, R. M. Lieder, T. Morek, T. Rzaca-Urban, H. Schnare, and W. Urban, Z. Phys. A **332**, 111 (1989).
[13] A. J. Kreiner, J. Davidson, M. Davidson, P. Thieberger, E. K. Warburton, S. Andre, and J. Genevey, Nucl. Phys. **A489**, 525 (1988).
[14] A. J. Larabee, M. P. Carpenter, L. L. Riedinger, L. H. Courtney, J. C. Waddington, V. P. Janzen, W. Nazarewicz, J. Y. Zhang, R. Bengtsson, and G. A. Leander, Phys. Lett. **B169**, 21 (1986).

[15] V. P. Janzen, Z. M. Liu, M. P. Carpenter, L. H. Courtney, H. Q. Jin, A. J. Larabee, L. L. Riedinger, J. K. Johansson, D. G. Popescu, J. C. Waddington, S. Monaro, S. Pilotte, and F. Donau, Phys. Rev. C **45**, 613 (1992).
[16] B. Roussiére, P. Kilcher, F. Le Blanc, J. Oms, J. Sauvage, H. Dautet, and ISOCELE Collaboration, Nucl. Phys. **A548**, 227 (1992).
[17] B. E. Gnade, R. W. Fink, and J. L. Wood, Nucl. Phys. **A406**, 29 (1983).
[18] A. Ben Braham, V. Berg, C. Bourgeois, P. Kilcher, J. Letessier, M. G. Desthuilliers-Porquet, C. Schck, A. Huck, A. Knipper, la Collaboration ISOLDE, C. Richard-Serre, and A. Höglund, Nucl. Phys. **A332**, 397 (1979).
[19] M. Piiparinen, J. C. Cunnane, P. J. Daly, C. L. Dors, F. M. Bernthal, and T. L. Khoo, Phys. Rev. Lett. **34**, 1110 (1975).
[20] M. C. Abreu, C. Bourgeois, P. Kilcher, M. G. Porquet, B. Roussiére, and J. Sauvage, Univ. Paris, Inst. Phys. Nucl. 1987 Ann. Rept., p.E17 (1988).
[21] K. Furuno, M. Oshima, T. Komatsubara, K. Furutaka, T. Hayakawa, M. Kedera, Y. Hatsukawa, M. Matsuda, S. Mitarai, T. Shizuma, T. Saitoh, N. Hashimoto, H. Kusakari, M. Sugawara, and T. Morikawa, Nucl. Instrum. Methods A **421**, 211 (1999).
[22] S. Juutinen, P. Ahonen, J. Hattula, R. Julin, A. Pakkanen, A. Virtanen, J. Simpson, R. Chapman, D. Clarke, F. Khazaie, J. Lisle, and J. N. Mo, Nucl. Phys. **A526**, 346 (1991).
[23] R. Bengtsson and S. Frauendorf, Nucl. Phys. **A327**, 139 (1979).
[24] W. Nazarewicz, R. Wyss, and A. Johnson, Phys. Lett. **B225**, 208 (1989).
[25] W. Nazarewicz, J. Dudek, R. Bengtsson, and I. Ragnarsson, Nucl. Phys. **A435**, 397 (1985).
[26] W. Satula and R. Wyss, Phys. Rev. C **50**, 2888 (1994).
[27] F. R. Xu, W. Satula, and R. Wyss, Nucl. Phys. **A669**, 119 (2000).
[28] W. Satula, R. Wyss, and P. Magierski, Nucl. Phys. **A578**, 45 (1994).
[29] F. R. Xu, P. M. Walker, J. A. Sheikh, and R. Wyss, Phys. Lett. **B435**, 257 (1998).
[30] S. K. Saha, M. Piiparinen, J. C. Cunnane, P. J. Daly, C. L. Dors, T. L. Khoo, and F. M. Bernthal, Phys. Rev. C **15**, 94 (1977).
[31] T. Kutsarova, C. Schuck, E. Gueorguieva, A. Minkova, I. Zartova, F. Hannachi, A. Korichi, and A. Lopez-Martens, Eur. Phys. J. **A23**, 69 (2005).
[32] I. G. Bearden, R. V. F. Janssens, M. P. Carpenter, E. F. Moore, I. Ahmad, P. J. Daly, R. Mayer, M. W. Drigert, P. B. Fernandez, B. Fornal, U. Garg, Z. W. Grabowski, T. L. Khoo, T. Lauritsen, W. Reviol, and D. Ye, Nucl. Phys. **A576**, 441 (1994).
[33] D. Ye, K. B. Beard, U. Garg, R. V. F. Janssens, M. P. Carpenter, I. Ahmad, T. L. Khoo, E. F. Moore, F. L. H. Wolfs, Ph. Benet, Z. W. Grabowski, and M. W. Drigert, Nucl. Phys. **A537**, 207 (1992).
[34] H. Hübel, A. P. Byrne, S. Ogaza, A. E. Stuchbery, G. D. Dracoulis, and M. Guttormsen, Nucl. Phys. **A453**, 316 (1986).
[35] T. Kutsarova, C. Schuck, E. Gueorguieva, A. Minkova, I. Zartova, F. Hannachi, A. Korichi, and A. Lopez-Martens, Eur. Phys. J. A **23**, 69 (2005).
[36] Y. H. Zhang, T. Hayakawa, M. Oshima, J. Katakura, Y. Hatsukawa, M. Matsuda, H. Kusakari, M. Sugawara, T. Komatsubara, and K. Furuno, Phys. Rev. C **65**, 014302 (2002).
[37] J. Nyberg, A. Johnson, M. P. Carpenter, C. R. Bingham, L. H. Courtney, V. P. Janzen, S. Juutinen, A. J. Larabee, Z. M. Liu, L. L. Riedinger, C. Baktash, M. L. Halbert, N. R. Johnson, I. Y. Lee, Y. Schutz, J. C. Waddington, and D. G. Popescu, Nucl. Phys. **A511**, 92 (1990).
[38] M. J. A. DE Voigt, R. Kaczarowski, H. J. Riezebos, R. F. Noorman, J. C. Bacelar, M. A. Deleplanque, R. M. Diamond, and F. S. Stephens, Nucl. Phys. **A507**, 447 (1990).
[39] F. Dönau and S. Frauendorf, Proc. Conf. on High angular momentum properties of nuclei, Oak Ridge, 1982, edited by N. R. Johnson (Harwood Academic, New York, 1983), p. 143.
[40] A. J. Larabee, L. H. Courtney, S. Frauendorf, L. L. Riedinger, J. C. Waddington, M. P. Fewell, N. R. Johnson, I. Y. Lee, and F. K. McGowan, Phys. Rev. C **29**, 1934 (1984).
[41] T. Shizuma, S. Mitarai, G. Sletten, R. A. Bark, N. L. Gjorup, H. J. Jensen, M. Piiparinen, J. Wrzesinski, and Y. R. Shimizu, Phys. Rev. C **69**, 024305 (2004).
[42] C. Wheldon, P. M. Walker, P. H. Regan, T. Saitoh, N. Hashimoto, G. Sletten, and F. R. Xu, Phys. Rev. C **59**, R2334 (1999).
[43] R. M. Lieder, H. Beuscher, W. F. Davidson, A. Neskakis, and C. Mayer-Boricke, Nucl. Phys. **A248**, 317 (1975).
[44] K. Neergard, P. Vogel, and M. Radomski, Nucl. Phys. **A238**, 199 (1975).
[45] H. Toki, K. Neergard, P. Vogel, and A. Faessler, Nucl. Phys. **A279**, 1 (1977).
[46] G. D. Dracoulis, B. Fabricius, R. A. Bark, A. E. Stuchbery, D. G. Popescu, and T. Kibedi, Nucl. Phys. **A510**, 533 (1990).
[47] G. J. Lampard, A. E. Stuchbery, and H. H. Bolotin, Nucl. Phys. **A536**, 397 (1992).